# Natural variation in the sequestosome-related gene, *sqst-5*, underlies zinc homeostasis in *Caenorhabditis elegans*

Kathryn S. Evans[1,2], Stefan Zdraljevic[1,2,#a], Lewis Stevens[1], Kimberly Collins[1], Robyn E. Tanny[1], Erik C. Andersen[1,3*]

[1]Molecular Biosciences, Northwestern University, Evanston, IL

[2]Interdisciplinary Biological Sciences Program, Northwestern University, Evanston, IL

[3]Robert H. Lurie Comprehensive Cancer Center, Northwestern University, Chicago, IL

[#a]Current address: Department of Human Genetics and HHMI, University of California, Los Angeles, CA

*** Corresponding author:**

E-mail: erik.andersen@northwestern.edu (ECA)

## Abstract

Zinc is an essential trace element that acts as a co-factor for many enzymes and transcription factors required for cellular growth and development. Altering intracellular zinc levels can produce dramatic effects ranging from cell proliferation to cell death. To avoid such fates, cells have evolved mechanisms to handle both an excess and a deficiency of zinc. Zinc homeostasis is largely maintained via zinc transporters, permeable channels, and other zinc-binding proteins. Variation in these proteins might affect their ability to interact with zinc, leading to either increased sensitivity or resistance to natural zinc fluctuations in the environment. We can leverage the power of the roundworm nematode *Caenorhabditis elegans* as a tractable metazoan model for quantitative genetics to identify genes that could underlie variation in responses to zinc. We found that the laboratory-adapted strain (N2) is resistant and a natural isolate from Hawaii (CB4856) is sensitive to micromolar amounts of exogenous zinc supplementation. Using a panel of recombinant inbred lines, we identified two large-effect quantitative trait loci (QTL) on the left arm of chromosome III and the center of chromosome V that are associated with zinc responses. We validated and refined both QTL using near-isogenic lines (NILs) and identified a naturally occurring deletion in *sqst-5,* a sequestosome-related gene, that is associated with resistance to high exogenous zinc. We found that this deletion is relatively common across strains within the species and that variation in *sqst-5* is associated with zinc resistance. Our results offer a possible mechanism for how organisms can respond to naturally high levels of zinc in the environment and how zinc homeostasis varies among individuals.

## Author summary

Zinc, although an essential metal, can be toxic if organisms are exposed to concentrations that are too high or too low. To prevent toxicity, organisms have evolved mechanisms to regulate zinc uptake from the environment. Here, we leveraged genetic variation between two strains of the roundworm *Caenorhabditis elegans* with different responses to high exogenous zinc to identify genes that might be involved in maintaining proper zinc levels. We identified four loci that contributed to differential zinc responses. One of these loci was the sequestosome-related gene *sqst-5*. We discovered that targeted deletions of *sqst-5* caused an increase in resistance to zinc. Although SQST-5 contains a conserved zinc-binding protein domain, it has yet to be directly implicated in the *C. elegans* zinc response pathway. We identified two common forms of genetic variation in *sqst-5* among 328 distinct strains, suggesting that variation in *sqst-5* must have emerged multiple times, perhaps in response to an environment of high zinc. Overall, our study suggests a natural context for the evolution of zinc response mechanisms.

# Introduction

Heavy metals such as zinc, iron, and copper are known to play important roles in many biological systems [1,2]. Of these metals, zinc is the most abundant and is essential for proper function of many proteins, including enzymes and transcription factors [3]. In addition to its function as a cofactor, zinc can act as a signaling molecule in neurons [4–7] and is known to play a role in cell-fate determination [8–12]. Because of its many functions, zinc deficiency has been shown to cause major defects, including growth inhibition and death in several species [8,13–16]. On the other hand, excess zinc can also be toxic, displaying phenotypic effects similar to copper deficiency, anemia, and neutropenia [17]. Although the exact mechanisms are unknown, the data suggest that excess zinc might bind ectopically to other proteins, displacing similar metals such as copper or magnesium from these proteins [8]. Because of this need for intracellular zinc balance even though environmental zinc might fluctuate, biological systems must use proper zinc homeostasis mechanisms for uptake, distribution, efflux, and detoxification [13].

The nematode *Caenorhabditis elegans* is a tractable metazoan model for studying the molecular mechanisms of zinc homeostasis and toxicity [8,18–20]. As observed in other organisms, zinc is essential for *C. elegans* growth [21]. In fact, it is estimated that about 8% of the *C. elegans* genes (1,600 genes) encode zinc-binding proteins [22]. However, zinc is also toxic to the nematode at higher concentrations [21]. High exogenous zinc can cause several defects including decreased growth rate and survival, suppression of the multivulva phenotype, and formation of bilobed lysosome-related organelles in intestinal cells [8]. Genetic screens have identified several genes that act to increase sensitivity to high levels of zinc (*haly-1*, *natc-1*, and *daf-21*) [8,23–26]. However, mutations in these genes cause a change in response to multiple stressors (including metals, heat, and oxidation), suggesting they are not specific to zinc homeostasis [8,25]. In addition to these nonspecific zinc proteins, *C. elegans* also has two complementary families (composed of 14 proteins each) of zinc transporters responsible for

maintaining constant intracellular zinc concentrations via import and export [8]. Four of these zinc exporters (*cdf-1*, *cdf-2*, *sur-7*, and *ttm-1*) have been shown to promote resistance to high zinc toxicity [8,9,21,23,27,28].

Although much is already known about zinc biology in *C. elegans*, previous studies were performed using a single laboratory-adapted strain (N2) that is known to differ significantly, both genetically and phenotypically, from wild isolates in the species [29]. As a complementary approach, we can leverage the power of natural genetic diversity among wild isolates [30–32] to identify novel mechanisms of zinc homeostasis and gain insights into the evolution of this process. We used a large panel of recombinant inbred advanced intercross lines (RIAILs) [33–35] constructed from a multi-generational cross between two genetically and phenotypically diverged strains, N2, the laboratory-adapted strain, and CB4856, a wild isolate from Hawaii [36]. This panel of RIAILs has been leveraged in several linkage mapping analyses, identifying hundreds of quantitative trait loci (QTL) [35,37–63]. In combination with a high-throughput phenotyping assay to measure animal length, optical density, and brood size [34], several quantitative trait genes (QTG) [35,63] and quantitative trait nucleotides (QTN) [41,42] underlying fitness-related traits have been described.

Here, we use linkage mapping analysis to identify four QTL in response to high exogenous zinc. Several genes previously identified to be involved in the zinc response were found within the QTL on chromosomes V and X. However, no known zinc-related genes were located in the large-effect chromosome III QTL, suggesting a potentially novel mechanism of zinc homeostasis. We constructed reciprocal near-isogenic lines (NILs) for each QTL and used them to validate the two large-effect QTL on chromosomes III and V. Expression QTL mapping and mediation analysis identified a single candidate gene, *sqst-5*, with predicted zinc ion-binding capability. We used CRISPR-Cas9 genome editing to show that strains without *sqst-5* were significantly more resistant to zinc supplementation than strains with a functional copy of *sqst-5*, suggesting a new role for this gene in zinc regulation. In addition to CB4856, several other wild isolates were found

to share a 111 bp deletion in *sqst-5*. Moreover, we identified a second group of strains with a distinct haplotype of variation at *sqst-5* that was also associated with zinc resistance. Together, these data suggest that the regulation of zinc in nematodes is complex, but binding and accumulation of excess zinc might be a mechanism to respond to exogenous zinc.

# Results

## Natural genetic variation in response to zinc is complex

We exposed four genetically divergent strains of *C. elegans* (N2, CB4856, JU258, and DL238) to increasing concentrations of exogenous zinc and measured their development (animal length, optical density, and normalized optical density) and reproductive ability (brood size) with a high-throughput assay using the COPAS BIOSORT (see Methods) [34,35,41–43]. In the presence of high concentrations of zinc, animals of all strains had smaller broods, shorter lengths, and were less optically dense compared to non-treated animals (**S1 Fig and S1 File**). Because nematodes grow longer and become more optically dense as they develop, these results suggest a zinc-induced developmental delay. Furthermore, the lower brood size of animals treated with zinc suggest that exogenous zinc hinders reproductive ability in some way. In addition to these overall trends, we also observed significant phenotypic variation among strains. For example, although all strains had smaller lengths in the presence of exogenous zinc, animals of the N2 strain were the largest (most resistant to zinc), and animals of the CB4856 strain were smaller (more sensitive to zinc). At 500 μM zinc, a concentration that both maximizes among-strain and minimizes within-strain phenotypic variation, we identified a substantial heritable genetic component for two highly correlated developmental traits: animal length ($H^2$ = 0.48, 95% CI [0.30, 0.61]) and optical density ($H^2$ = 0.48, 95% CI [0.28, 0.59]) (**S2 File**).

To investigate the genetic basis of zinc response, we exposed a panel of 253 RIAILs derived from a cross between the N2 and CB4856 strains (set 2 RIAILs, see Methods) to high

125 exogenous zinc (**S3 File**). In these conditions, the N2 animals were longer (**S2 Fig**) and more
126 optically dense (**Fig 1A**) than the CB4856 animals, and were thus more resistant to high zinc
127 supplementation. Interestingly, many of the RIAILs were either more resistant than N2 or more
128 sensitive than CB4856, suggesting that loci of opposite genotypes are either acting additively or
129 interacting in the RIAILs to produce the observed transgressive phenotypes [64]. Linkage
130 mapping analysis identified 12 QTL across all traits, representing five unique QTL on
131 chromosomes III, IV, V, and X (**S2 Fig and S4 File**). Because genetic architectures looked similar
132 across these traits, we chose to focus our analyses on optical density to avoid redundant analyses
133 of correlated traits (**Fig 1B**). Together, the four QTL underlying animal optical density explain
134 40.5% of the phenotypic variation among the RIAILs. As expected, QTL of opposite effects were
135 observed. Strains with the CB4856 allele on chromosome III were more resistant to zinc than
136 strains with the N2 allele at this locus. By contrast, strains with the CB4856 alleles on
137 chromosomes IV, V, and X were more sensitive to zinc than strains with the N2 alleles at these
138 loci (**Fig 1C, S3 and S4 Files**). We scanned the genome for interactions between pairs of genomic
139 markers that might affect the phenotypic distribution of the RIAIL panel and identified no
140 significant interactions (**S3 Fig and S5 File**). We further examined the additivity of the two QTL
141 with the largest and opposite effect sizes (QTL on chromosomes III and V). We concluded that
142 RIAILs with the CB4856 allele on chromosome III and the N2 allele on chromosome V were the
143 most resistant, and RIAILs with the N2 allele on chromosome III and the CB4856 allele on
144 chromosome V were the most sensitive (**S4 Fig and S3 File**). Furthermore, the effect size of the
145 chromosome III locus was similar regardless of the genotype on chromosome V (**S4 Fig and S3**
146 **File**), and no significant interaction term was identified using a linear model (ANOVA, $p = 0.251$).
147 These results suggest that multiple additive QTL rather than interacting loci affect animal optical
148 densities in zinc.
149

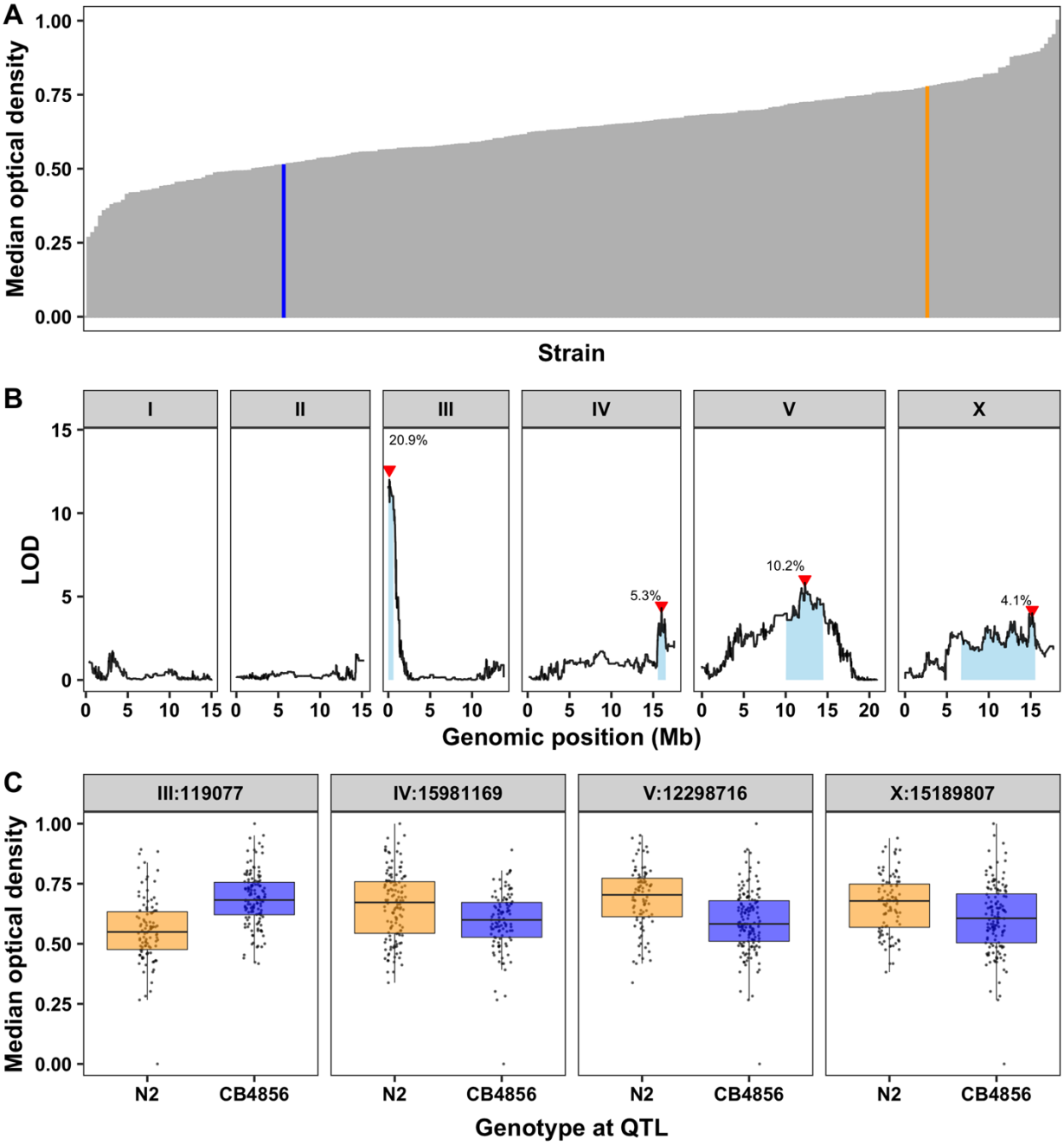


**Fig 1. Linkage mapping identifies four QTL in response to high dietary zinc. A)** Median optical densities (y-axis) of 253 RIAILs (x-axis) in response to zinc supplementation are shown. The parental strains are colored: N2, orange; CB4856, blue. **B)** Linkage mapping results for optical density (median.EXT) is shown. Genomic position (x-axis) is plotted against the logarithm of the odds (LOD) score (y-axis) for 13,003 genomic markers. Each significant QTL is indicated by a red triangle at the peak marker, and a blue rectangle shows the 95% confidence interval around the peak marker. The percentage of the total variance in the RIAIL population that can be explained by each QTL is shown above the QTL. **C)** For each QTL, the normalized residual median optical densities (y-axis) of RIAILs split by genotype at the marker with the maximum LOD score (x-axis) are plotted as Tukey box plots. Each point corresponds to a unique recombinant strain. Strains with the N2 allele are colored orange, and strains with the CB4856 allele are colored blue.

## Near-isogenic lines fractionate the chromosome V QTL into multiple additive loci

We first investigated whether any of the 28 known zinc transporters or any of the other 15 zinc-related genes [8] are located in one of the four detected QTL intervals. We discovered that three of these genes lie in the QTL on chromosome V and 11 lie in the QTL on chromosome X (**S6 File**). However, none of these zinc-related genes lie in either of the QTL on chromosomes III or IV (**S6 File**). To isolate and validate the effect of these four QTL, we constructed reciprocal near-isogenic lines (NILs) by introgressing a genomic region surrounding each of the QTL from the CB4856 strain into the N2 genetic background or vice versa (**S7 and S8 Files**). We then measured the animal optical densities in the presence of zinc for these strains to provide experimental evidence in support of each QTL independently. For the three QTL on chromosomes IV, V, and X, the N2 allele was associated with zinc resistance (**Fig 1C, S3 and S4 Files**). However, strains with the N2 allele crossed into a CB4856 genetic background on chromosomes IV and X were as sensitive as the CB4856 strain, and strains with the CB4856 allele crossed into an N2 genetic background were as resistant as the N2 strain (**S5 Fig, S9 and S10 Files**). These two QTL have the smallest effect sizes among the four QTL detected and each explain only 5% of the total phenotypic variation among the RIAILs. The lack of a significant difference between the NILs and their respective parental strains suggests that the QTL effect might be smaller than 5% and we were underpowered to detect the difference. Alternatively, the interval might contain QTL of opposing effects requiring additional smaller NILs.

By contrast, the NIL with the N2 allele surrounding the QTL on chromosome V introgressed into the CB4856 genetic background is significantly more resistant than the sensitive CB4856 strain (**S5 Fig, S9 and S10 Files**). This result confirms that genetic variation between the N2 and CB4856 strains on the center of chromosome V contributes to the differences in animal optical densities between the strains in the presence of high exogenous zinc. To further narrow this QTL, we created a panel of NILs with smaller regions of the N2 genome introgressed into the

CB4856 genetic background. We exposed a subset of these NILs to zinc and measured their optical densities. We found strains with the resistant N2 phenotype (ECA481; V:9.6-13.8 Mb), strains with the sensitive CB4856 phenotype (ECA411; V:11.3-13.9 Mb), and strains with an intermediate phenotype (ECA437; V:10.5-13.8 Mb) (**Fig 2, S10 and S11 Files**). These data imply the existence of at least two loci (V:9.6-10.5 Mb and V:10.5-11.3 Mb) at which the N2 allele confers resistance to zinc. The intermediate strain (ECA437) contains one N2 locus and one CB4856 locus, and the resistant strain (ECA481) contains two N2 loci. Because this region is in the center of a chromosome where recombination frequency is lower [33], we were unable to generate NILs with a breakpoint to further narrow the QTL. Furthermore, it is possible that multiple small-effect loci are contributing to each of the two QTL, rendering it difficult to identify each causal gene or variant. Regardless, at least two novel loci on chromosome V were identified that influence zinc sensitivity in *C. elegans*.

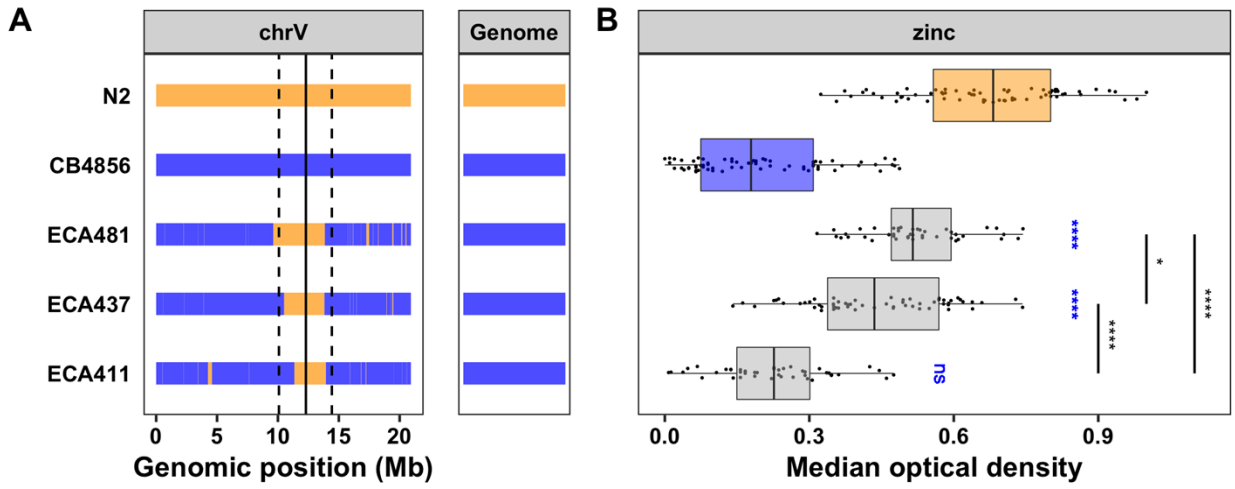


**Fig 2. NILs identify multiple QTL on chromosome V. A)** Strain genotypes are shown as colored rectangles (N2: orange, CB4856: blue) in detail for chromosome V (left) and in general for the rest of the chromosomes (right). The solid vertical line represents the peak marker of the QTL, and the dashed vertical lines represent the confidence interval. **B)** Normalized residual median optical density in zinc (median.EXT, x-axis) is plotted as Tukey box plots against strain (y-axis). Statistical significance of each NIL compared to CB4856 is shown above each strain (ns = non-significant (p-value > 0.05); *, **, ***, and *** = significant (p-value < 0.05, 0.01, 0.001, or 0.0001, respectively).

## Analysis of the chromosome III QTL suggests that a sequestosome-related gene, *sqst-5*, contributes to differences in zinc responses

The QTL on chromosome III accounts for 20% of the phenotypic variance in zinc response across the RIAIL population. In contrast to the previous three QTL, the CB4856 allele is associated with zinc resistance and the N2 allele is associated with zinc sensitivity (**Fig 1C, S3 and S4 Files**). The strain with the N2 allele on chromosome III crossed into a CB4856 genetic background (ECA859) was significantly more sensitive than the CB4856 strain (hyper-sensitive) and the strain with the opposite genotype (ECA838) was significantly more resistant than the N2 strain (hyper-resistant) (**S5 Fig, S9 and S10 Files**). These results demonstrate that this locus contributes to the observed transgressive phenotypes in the RIAILs (**Fig 1A, S3 File**). We also measured animal optical densities in zinc for individuals heterozygous for the chromosome III locus to determine whether the N2 or CB4856 allele confers the dominant phenotype. To analyze heterozygous individuals, we developed a modified high-throughput assay (see Methods, **S6 Fig, S12 File**). Individuals heterozygous for the chromosome III locus in the N2 genetic background (N2xECA838) were hyper-resistant similar to the NIL that is homozygous CB4856 for the chromosome III locus in the N2 genetic background (ECA838) (**Fig 3, S10 and S13 Files**). By contrast, individuals heterozygous for the chromosome III locus in the CB4856 genetic background (CB4856xECA859) were significantly more resistant than their hyper-sensitive NIL counterpart, which is homozygous N2 for the chromosome III locus in the CB4856 genetic background (ECA859). The phenotype of this heterozygous strain was also similar to that of the CB4856 strain. The results of these crosses validate that genetic variation between N2 and CB4856 on the left arm of chromosome III contributes to the nematode zinc response and indicate that the CB4856 allele conferred a dominant phenotype.

Because no previously identified zinc-related genes are in this interval, we investigated the composition of the genes in N2 to look for any obvious candidates that might underlie this

QTL. We found 119 genes in this interval (**Table 1, S13 File**). A change in phenotype is often observed when either genetic variation causes a change in the amino-acid sequence of the protein (protein-coding variation) or genetic variation causes a change in gene expression. Previously, whole-genome gene expression was measured in a set of 208 RIAILs derived from the N2 and CB4856 strains [50] and expression QTL (eQTL) mapping was performed [50,63]. We used this dataset to find genes with an eQTL that maps to our region of interest. In total, we eliminated 19 genes that had no genetic variation in CB4856 and prioritized 62 genes that had protein-coding variation and/or an eQTL that mapped to this region (**Table 1, S14 File**).

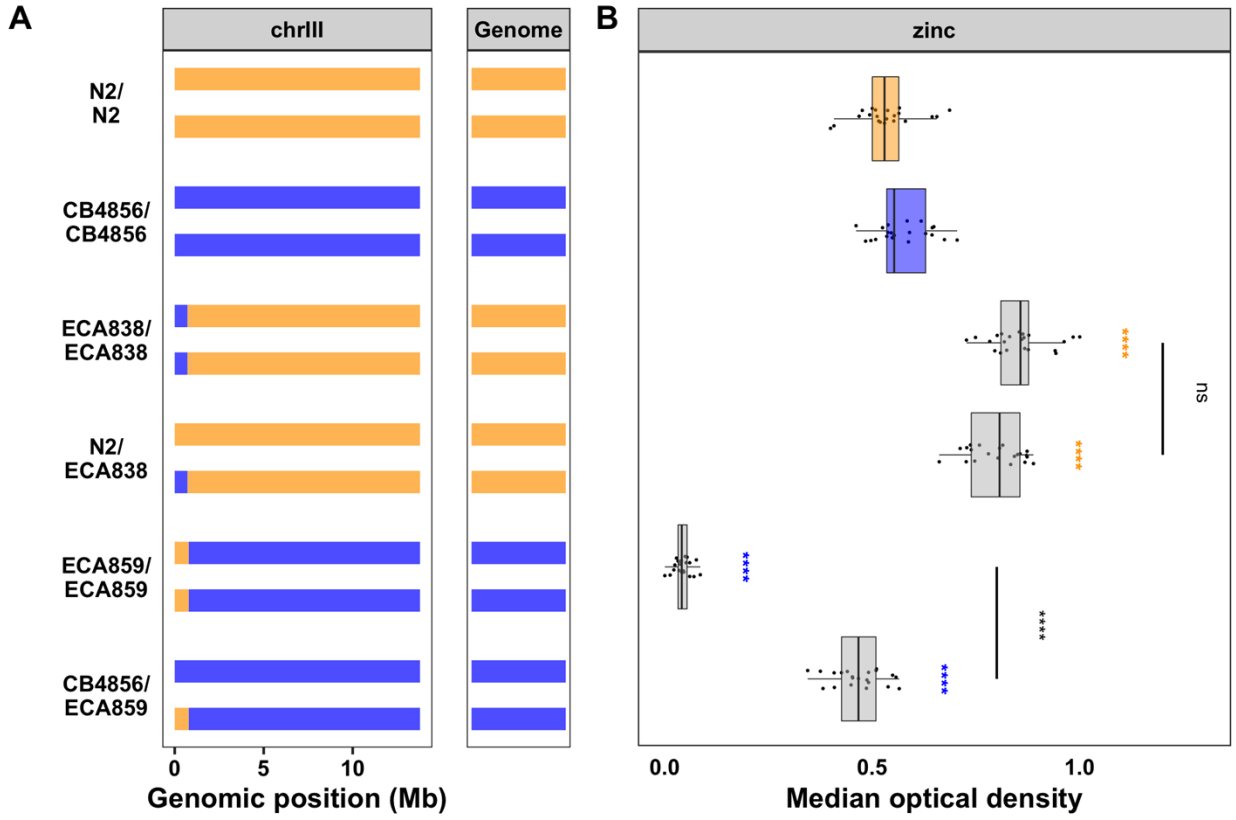


**Fig 3. Dominance of chromosome III QTL. A)** Strain genotypes are shown as colored rectangles (N2: orange, CB4856: blue) in detail for chromosome III (left) and in general for the rest of the chromosomes (right). Each rectangle represents a single copy of chromosome III. **B)** Normalized residual median optical density in zinc (median.EXT, x-axis) is plotted as Tukey box plots against strain (y-axis). The N2 strain, which is normally resistant to zinc, was sick in this experiment. Statistical significance of each strain compared to its parental strain (ECA838/ECA838 and N2/ECA838 to N2 and ECA859/ECA859 and CB4856/ECA859 to CB4856) is shown above each strain and colored by the parent strain it was tested against (ns = non-significant (p-value > 0.05); *, **, ***, and *** = significant (p-value < 0.05, 0.01, 0.001, or 0.0001, respectively).

**Table 1: Genes in QTL intervals for chromosomes III and V**

| QTL interval (bp) | No genetic variation[a] | Protein-coding variation and/or eQTL[b] | Other genetic variation[c] | Other eQTL that map to interval[d] | Total |
|---|---|---|---|---|---|
| **III:4,664-597,553** | 19 | 55 | 45 | 7 | **126** |
| **V:9,620,518-10,511,995** | 183 | 49 | 97 | 24 | **353** |
| **V:10,511,995-11,345,444** | 215 | 45 | 115 | 19 | **394** |

[a]Genes within genomic interval with no genetic variation
[b]Genes within genomic interval with protein-coding variation and/or an eQTL that maps to this interval
[c]Genes within genomic interval with non-protein-coding variation and no eQTL that maps to this interval
[d]Genes outside genomic interval with an eQTL that maps to this interval

To narrow our list of genes further, we analyzed the functional descriptions and gene ontology (GO) annotations for all 62 candidate genes. A gene that is predicted to bind zinc and has protein-coding variation or variation in gene expression between N2 and CB4856 would be a high-priority candidate. We identified four genes that are predicted to bind zinc and a fifth gene that is regulated by a zinc finger transcription factor (**S14 File**). Upon further inspection, one of these five genes (*sqst-5*) also had an eQTL that was originally assigned to the nearby pseudogene *ver-2* (**Fig 4A, S7 Fig and S15 File**). RIAILs with the N2 allele at the *sqst-5* locus have significantly higher expression of the gene than those with the CB4856 allele (**Fig 4B and S15 File**). We previously showed that mediation analysis can be a useful tool to link variation in gene expression with drug-response phenotypes [63]. We used the standard high-throughput assay to measure zinc responses for 121 of the 208 RIAILs with gene expression data (**S3 File**) and performed mediation analysis for each of the 17 genes with an eQTL in the region (**S16 File**). The mediation estimate for *sqst-5* was the strongest hit (**Fig 4C**). Together, these results suggest that genetic variation on chromosome III causes a decrease in expression of *sqst-5* that leads to increased zinc resistance.

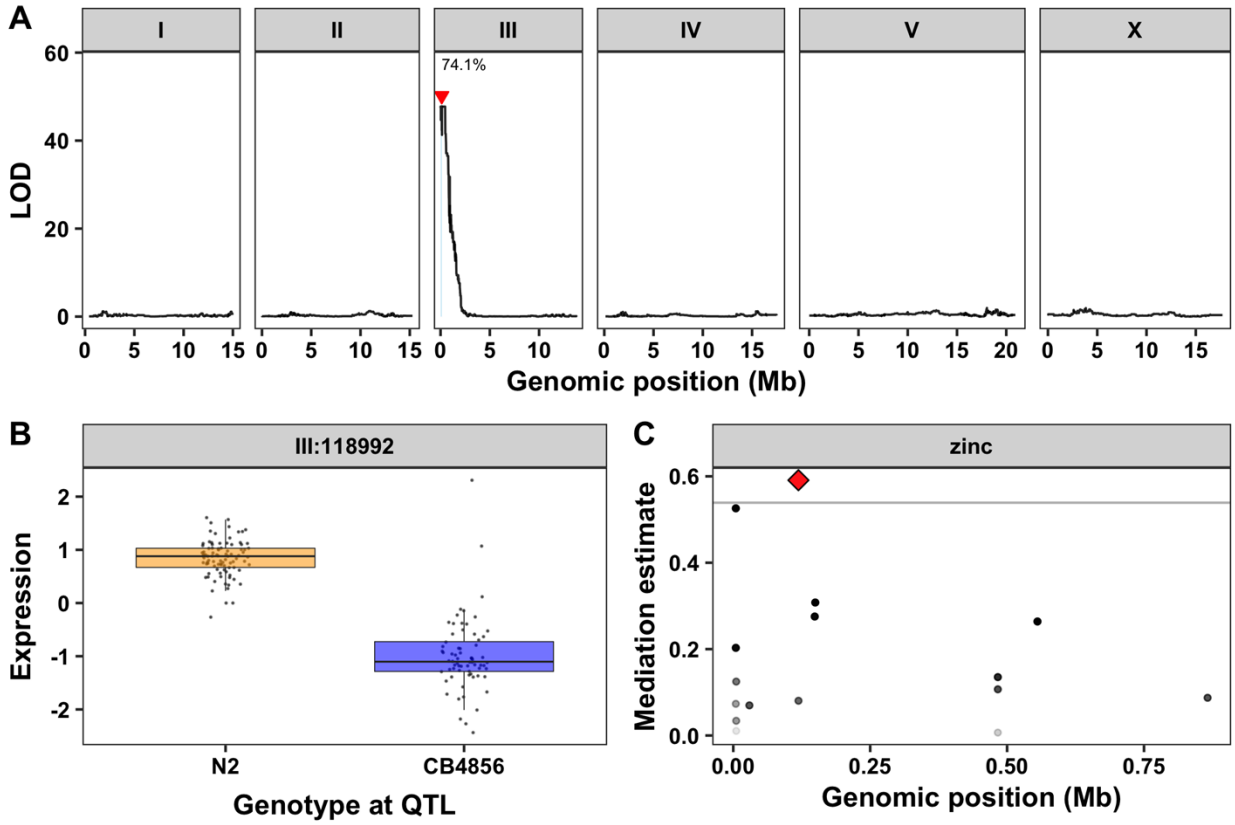


**Fig 4. Expression QTL mapping and mediation analysis for *sqst-5*. A)** Results from the linkage mapping using expression of *sqst-5* as a quantitative trait. Genomic position (x-axis) is plotted against the logarithm of the odds (LOD) score (y-axis) for 13,003 genomic markers. The significant QTL is indicated by a red triangle at the peak marker, and a blue rectangle shows the 95% confidence interval around the peak marker. The percentage of the total variance in the RIAIL population that can be explained by the QTL is shown above the QTL. **B)** The expression of *sqst-5* (y-axis) of RIAILs split by genotype at the marker with the maximum LOD score (x-axis) are plotted as Tukey box plots. Each point corresponds to a unique recombinant strain. Strains with the N2 allele are colored orange, and strains with the CB4856 allele are colored blue. **C)** Mediation estimates calculated as the indirect effect that differences in expression of each gene plays in the overall phenotype (y-axis) are plotted against genomic position of the eQTL (x-axis) on chromosome III for al 17 genes with an eQTL in the drug-response QTL confidence interval. The 95th percentile of the distribution of mediation estimates is represented by the horizontal grey line. The confidence of the estimate increases (p-value decreases) as points become more solid. *sqst-5* is represented by a red diamond.

## Variation in *sqst-5* underlies differences in zinc responses

To test the function of *sqst-5* in the zinc response, we constructed two independently derived strains harboring large deletions of *sqst-5* in both the N2 and CB4856 genetic backgrounds. Because RIAILs with the CB4856 allele (which was associated with higher resistance to zinc) have lower expression of *sqst-5* (**Fig 4B and S15 File**), we expected *sqst-5*

297 deletions in the CB4856 genetic background might cause little or no change in zinc resistance.
298 Alternatively, we expected *sqst-5* deletions in the N2 genetic background might cause increased
299 zinc resistance. Surprisingly, we found that deletions of *sqst-5* had no effect in either background
300 (**S8 Fig, S10 File and S17 Files**). However, the increased sensitivity of the N2 allele in the
301 CB4856 genetic background (ECA859) always had a much larger effect than the increased
302 resistance of the CB4856 allele in the N2 background (ECA838) (**Fig 3, S5 Fig, S9- S10 and S13**
303 **Files**). To take advantage of this sensitization, we deleted *sqst-5* in the hyper-sensitive NIL strain
304 that contains the N2 *sqst-5* allele in the CB4856 genetic background (ECA859). We hypothesized
305 that deleting *sqst-5* in the hyper-sensitive NIL would make this strain less sensitive to zinc (more
306 similar to the CB4856 phenotype). As expected, we observed a significant increase in resistance
307 for these deletions compared to the NIL (**S9 Fig, S10 and S18 Files**), indicating a role for *sqst-5*
308 in the *C. elegans* zinc response.

309 To provide further evidence that natural variation between N2 and CB4856 in *sqst-5*
310 underlies the chromosome III QTL, we measured the optical density of individuals hemizygous
311 for the N2 *sqst-5* allele in the hyper-sensitive NIL genetic background (ECA2517xECA859) in
312 response to zinc. If a loss-of-function allele of *sqst-5* in the CB4856 strain is responsible for the
313 variation in zinc response between N2 and CB4856 (**S8 Fig, S10 and S17 Files**), then this
314 hemizygous strain should show the same sensitivity as both the CB4856 strain and the strain with
315 the homozygous deletion of *sqst-5* in the hyper-sensitive NIL genetic background (ECA2517). We
316 observed that the strain hemizygous for the N2 *sqst-5* allele was indeed more resistant than the
317 hyper-sensitive NIL and similar in sensitivity to the CB4856 strain (**Fig 5, S10 and S19 Files**).
318 This result recapitulated the result of the dominance assay (**Fig 3**), suggesting that a loss-of-
319 function allele of *sqst-5* conferred a dominant resistance phenotype. A dominant phenotype
320 caused by a loss-of-function allele is, most times, caused by haploinsufficiency. Therefore, the
321 zinc-response phenotype driven by the single functional N2 *sqst-5* allele is not sufficient to
322 produce the hyper-sensitive phenotype of the NIL with two functional N2 alleles.

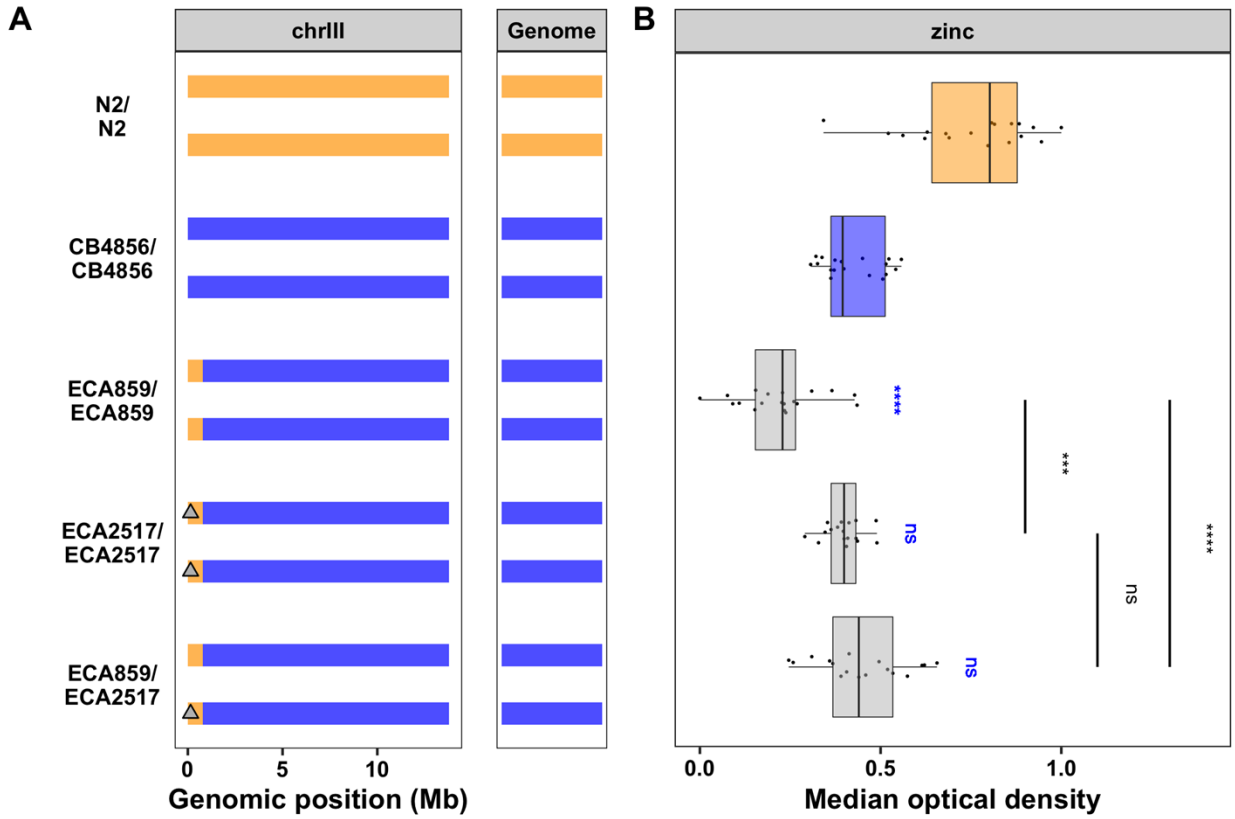


**Fig 5. The gene *sqst-5* confers zinc sensitivity. A)** Strain genotypes are shown as colored rectangles (N2: orange, CB4856: blue) in detail for chromosome III (left) and in general for the rest of the chromosomes (right). Each rectangle represents a single copy of chromosome III, and grey triangles represent *sqst-5* deletions. **B)** Normalized residual median optical density in zinc (median.EXT, x-axis) is plotted as Tukey box plots against strain (y-axis). The N2 strain, which is normally resistant to zinc, was sick in this experiment. Statistical significance of each strain compared to CB4856 is shown above each strain and NIL pairwise significance is shown as a bar above strains (ns = non-significant (p-value > 0.05); *, **, ***, and *** = significant (p-value < 0.05, 0.01, 0.001, or 0.0001, respectively).

## A natural deletion in *sqst-5* is conserved across wild isolates

We next searched for specific genetic variants in *sqst-5* that could lead to a loss-of-function allele in CB4856. We investigated the sequence read alignments of the N2 and CB4856 strains at the *sqst-5* locus using the Variant Browser on CeNDR (elegansvariaton.org) [32] and observed a putative large deletion in the second exon. We confirmed that this deletion is 111 bp (N2 coordinates: chrIII:147,076-147,186 bp) using a whole-genome alignment between the N2 reference genome and the CB4856 genome recently assembled using long-read sequencing [65]

(**Fig 6**, **S20 and S21 Files**). We ran gene prediction algorithms on the CB4856 sequence, but no gene was predicted (**S22 File**). The SQST-5 protein in the N2 strain has a single characterized protein domain: a Zinc finger, ZZ-type (Wormbase.org, WS275). The ZZ-type domains are predicted to bind two zinc ions using a repeated conserved motif of Cys-X2-Cys and are also important for protein-protein interactions [66,67]. Interestingly, when we overlaid the location of the ZZ-type domain with the CB4856 alignment, we discovered that the 111 bp deletion spans most of the ZZ-type domain, including the essential Cys-X2-Cys motif (**Fig 6A**). Because this domain is important for binding zinc ions, this result suggests that even if CB4856 expresses low levels of SQST-5, it is unlikely to bind zinc at the same level as strains with a complete ZZ-type domain.

We next investigated structural variation across a panel of 328 wild isolates to ask if this deletion is unique to the CB4856 strain or common across many wild strains. We identified 31 additional strains with the same 111 bp deletion as CB4856 by manual inspection using the Variant Browser on CeNDR (**S23 File**). We also identified 25 strains that harbored low sequence identity with the N2 reference genome, indicating that these strains might contain structural variation different from the deletion in the CB4856 strain. We assessed the genetic relatedness of these strains by constructing a neighbor-joining tree for all 328 wild isolates using the single nucleotide variants near and within *sqst-5* (**S24 File**). All 32 strains with the predicted deletion in *sqst-5* cluster together (**Fig 6B**), suggesting these strains inherited this deletion from a common ancestor. These strains were not isolated from a single location, but rather spread geographically across Europe and the Pacific Rim (**S10 Fig and S23 File**). Furthermore, 24 of the 25 strains with other putative structural variation in *sqst-5* also cluster together separately from the strains with the 111 bp deletion (**Fig 6B and S24 File**). This result suggests that this second group of strains also share a common ancestor that harbored variation in *sqst-5*. Additionally, strains with the deletion and strains with the other haplotype are sometimes found in nearby locations (**S10 Fig**

366 **and S23 File**). Regardless, the 111 bp deletion and putative other structural variants might cause
367 loss of *sqst-5* function.

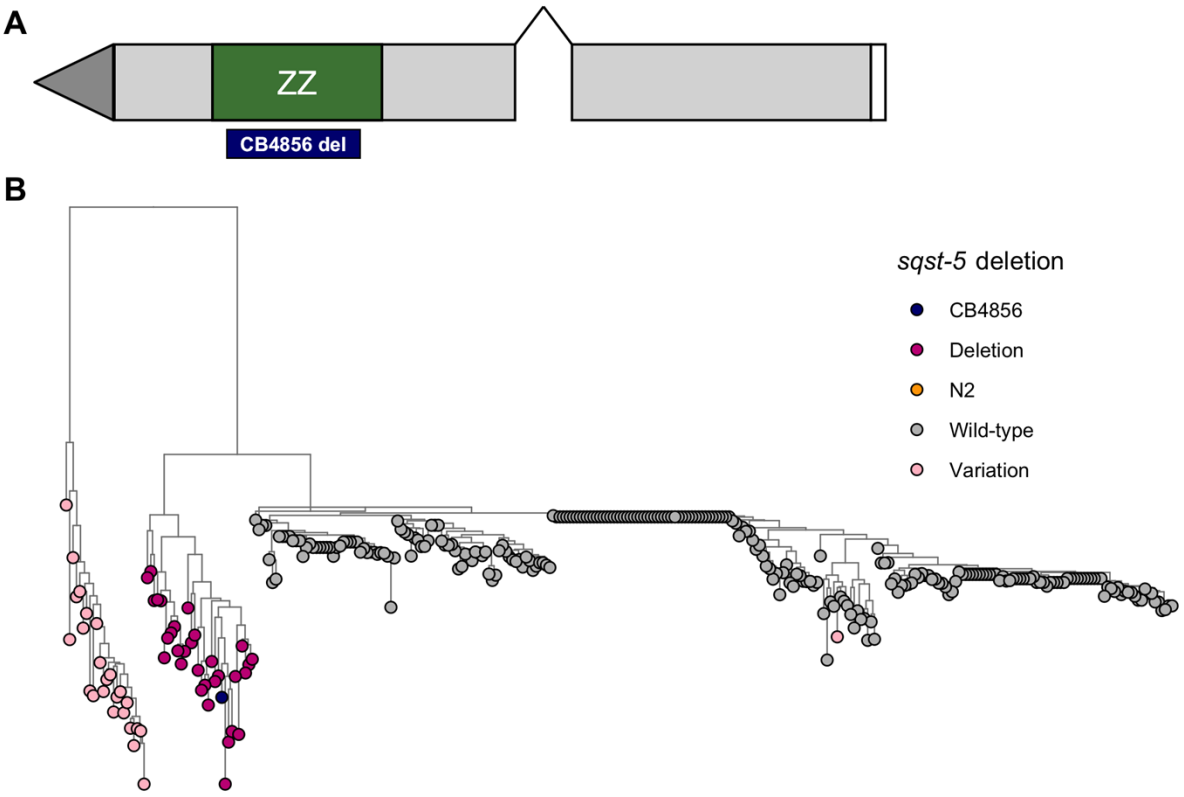


368
369

370 **Fig 6. Natural genetic variation in *sqst-5*. A)** Gene model of *sqst-5*. Grey rectangles represent exons,
371 and connecting black lines represent introns. The ZZ-type domain is indicated by a green rectangle, and
372 the location of the natural 111 bp deletion in CB4856 is indicated below with a blue rectangle. **B)** Neighbor-
373 joining tree indicating genetic relatedness between wild isolates at the *sqst-5* locus. Branch lengths indicate
374 the rate, the tree is midpoint rooted. Tips are colored by the variation haplotype at *sqst-5*: (Wild-type: grey,
375 N2: orange, CB4856: navy, Deletion: magenta, Other putative structural variation: light pink).
376
377 To test if a loss-of-function allele of *sqst-5* correlates with zinc resistance among our panel
378 of wild isolates, we measured animal development (length, optical density, and normalized optical
379 density) and reproductive ability (brood size) of 81 strains in response to zinc (**S25 File and S25**
380 **File**). Including CB4856, we tested nine strains with variation in *sqst-5*: four strains with the 111
381 bp deletion and five strains with the other putative structural variation. On average, these nine
382 strains were more resistant than the rest of the population (**Fig 7A, S11 Fig and S26 File**), and
383 variation in *sqst-5* explained up to 11.5% (median.EXT; *p-value = 0.0019*) of the total variation in

384 zinc responses among the wild isolates. Genome-wide association mapping identified eight small-
385 effect QTL across the four zinc-response traits (**S11 Fig**). One trait, normalized optical density,
386 had a QTL on the left arm of chromosome III (**Figs 7B-C**). The proximity of this QTL to *sqst-5*
387 suggests that natural variation in *sqst-5* likely also contributes to variation in response to zinc
388 among a panel of wild *C. elegans* strains.
389
390

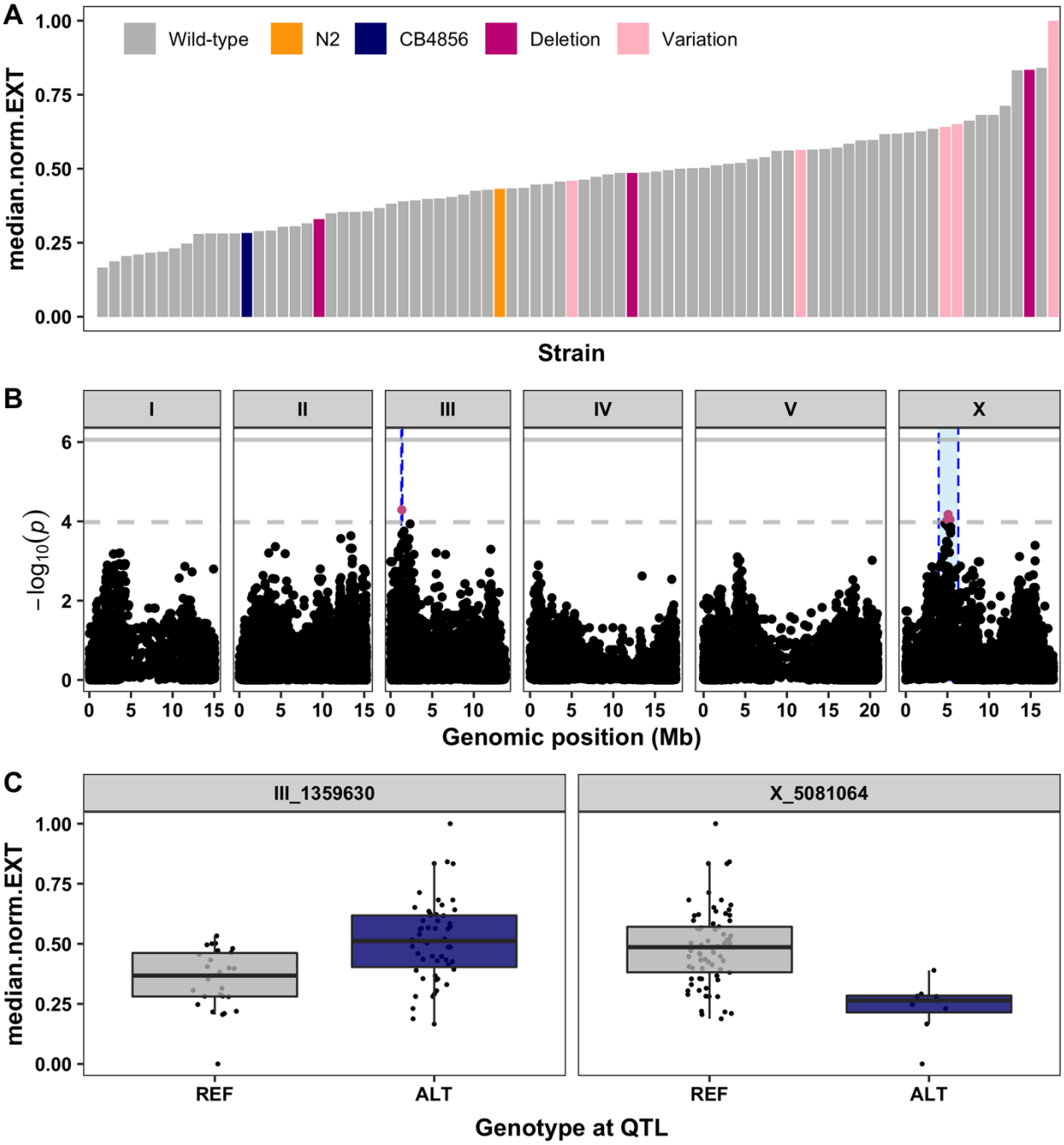


**Fig 7**. **Genome-wide association (GWA) mapping suggests common variation at *sqst-5* is associated with differences in zinc responses among wild isolates. A)** Normalized residual median normalized optical density (median.norm.EXT, y-axis) of 81 wild isolates (x-axis) in response to zinc supplementation. Strains are colored by the parental strains N2 (orange) and CB4856 (blue) or by the *sqst-5* variation (Deletion: magenta, other variation: light pink) **B)** GWA results are shown. Genomic position (x-axis) is plotted against the *-log10(p)* value (y-axis) for each SNV. SNVs are colored pink if they pass the genome-wide eigen-decomposition significance threshold designated by the dotted grey line. The solid grey line represents the more stringent Bonferroni significance threshold. The genomic regions of interest that pass the significance threshold are highlighted by blue rectangles. **C)** For each QTL, the normalized residual median normalized optical density (median.norm.EXT, y-axis) of strains split by genotype at the peak marker (x-axis) are plotted as Tukey box plots. Each point corresponds to a wild isolate strain. Strains with

403 the N2 reference allele are colored grey, and strains with an alternative allele are colored navy.
404

405 # Discussion

406 We used linkage mapping to identify four QTL in response to high levels of exogenous
407 zinc. We validated the two QTL with the largest effects on chromosomes III and V using near-
408 isogenic lines. The QTL on chromosome V was further dissected into at least two additive loci
409 that became difficult to narrow further. Mediation analysis was performed for the genes with
410 expression variation that overlaps with the QTL on chromosome III, and a single gene (*sqst-5*)
411 was identified whose variation in expression between N2 and CB4856 is correlated with
412 differences in responses to zinc. The CB4856 strain harbors a natural deletion of this gene. We
413 deleted the N2 version of *sqst-5* using CRISPR-Cas9 genome editing and showed that strains
414 without *sqst-5* were significantly more resistant to exogenous zinc than strains with a functional
415 copy of *sqst-5*, suggesting a new role for *sqst-5* in zinc homeostasis. In addition to CB4856,
416 several other wild isolates were found to have a putative independent structural variant in *sqst-5*
417 that is loosely correlated with resistance to zinc. These strains cluster genetically into two distinct
418 groups, suggesting that functional variation in *sqst-5* has emerged multiple times. These results
419 demonstrate the power of leveraging natural genetic variation to identify novel genes in a toxin-
420 response pathway and suggest mechanisms for how high exogenous zinc can be mitigated in
421 natural environments.

422

423 ## A complex genetic architecture underlies differences in zinc responses

424 The identification of multiple QTL in response to excess zinc is not surprising, as zinc is
425 an essential trace element and up to 8% of *C. elegans* genes have been predicted to encode
426 proteins that bind zinc [22]. In particular, 28 genes encode putative zinc transporters and an
427 additional 15 genes have been identified via mutagenesis screens in N2 that promote either zinc
428 resistance or sensitivity [8,18]. We identified two QTL that contain at least one gene that was

previously found to be involved in the nematode zinc response and an additional two QTL that do not contain any genes previously found to affect zinc responses (**S6 File**). Several of the genes with previously described roles in the zinc response are located on chromosome X. However, only three of these genes (*hke-4.2*, *hizr-1*, and *elt-2*) have protein-coding variation in CB4856. The results of the linkage mapping experiment (**Fig 1B**) identified a broad peak on chromosome X, but we were unsuccessful validating this QTL using NILs (**S5 Fig**) likely because the QTL could contain multiple small-effect loci that could each act in opposite directions. By contrast, we were able to validate that genetic variation on chromosome V contributes to the nematode zinc responses (**Fig 2**). However, as more NILs were tested with smaller introgressions, we observed a fractionation of the QTL into at least two small-effect loci. Several previous studies that aimed to deeply validate a single QTL have instead identified many tightly linked antagonistic QTL underlying the major QTL [49,68–75]. Unfortunately, as each QTL fractionates into several QTL, the individual effect sizes become smaller and our ability to accurately interpret signal from noise becomes more difficult. This polygenic nature of complex traits is a major roadblock in going from QTL to QTG [76–78].

Although we were unable to identify specific genes on chromosome V that contribute to the nematode zinc response, we were able to narrow the QTL interval from 4.3 Mb (chrV:10,084,029-14,428,285) to 1.2 Mb (chrV:10,084,029-11,345,444) containing at least two loci that underlie differential responses to zinc. Of the 573 genes of interest (**Table 1**), we identified two high-priority candidate genes (*zhit-3* and *H27A22.1*) that are predicted to bind zinc and have protein-coding variation in the CB4856 strain. The gene *zhit-3* encodes a protein that is an ortholog of the human protein ZNHIT6 and contains a zinc finger HIT-type domain (Wormbase.org, WS275). The gene *H27A22.1* encodes a protein that is an ortholog of the human protein QPCTL with glutaminyl-peptide cyclotransferase (Wormbase.org, WS275). It is possible that genetic variation in one or both of these genes underlies the QTL on chromosome V.

454 However, future studies are needed to confirm the role of these genes in the nematode zinc
455 response.

456 Although zinc is the most biologically relevant heavy metal, other divalent cations with
457 similar chemistries also play important roles in biological systems (copper, nickel, and iron) or are
458 highly toxic (cadmium) [1,2,8]. We previously performed linkage mapping for three of these heavy
459 metals and found that QTL for zinc, copper, and nickel overlap on the right arm of chromosome
460 IV (**S12 Fig and S27 File**) [43,75]. The overlap of this QTL with other heavy metal QTL suggest
461 that perhaps the molecular mechanisms underlying these QTL are not specific to zinc.
462 Furthermore, this QTL is in regions previously defined as a QTL hotspot where a single pleiotropic
463 gene might control several toxin responses or several independent yet tightly linked genes might
464 control different traits [43]. Regardless, the high-effect QTL on chromosome III seems to be
465 unique to the zinc response, as none of the other metals have a QTL on chromosome III (**S12**
466 **Fig**).

467

468 **Common genetic variation underlies differential responses to exogenous zinc**

469 We discovered 31 additional wild strains with the same 111 bp deletion in *sqst-5* as found
470 in the CB4856 strain and another 25 strains that show evidence of different structural variation.
471 Long-read sequencing and local genome assembly of strains with this alternative variation are
472 needed to fully define these haplotypes. Although these strains were isolated globally (**S10 Fig**),
473 phylogenetic analysis suggests that these strains comprise two common classes of variation at
474 the *sqst-5* locus (**Fig 6B**). Strains from these two classes of variation are sometimes found in
475 close geographical proximity, indicating a possibility for convergent evolution in zinc resistance,
476 perhaps in geographic regions with high levels of zinc in the environment. We require further
477 investigation of metal contents in niches that contain *C. elegans* to connect environmental zinc
478 levels to natural genetic variation.

We measured zinc responses for a subset of wild strains and found that variation in *sqst-5* could explain 11.5% of the total variation in response to zinc among the panel of wild isolates. Interestingly, N2 and CB4856 were among the more sensitive strains tested (**Fig 7 and S11 Fig**), suggesting the existence of several loci not found within the CB4856 strain that influence zinc responses. GWA mapping discovered several small-effect loci across the genome that were associated with zinc resistance or sensitivity (**S11 Fig**). In particular, the QTL on chromosome III (nearby the *sqst-5* locus) and chromosome X overlapped with QTL discovered using linkage mapping. Alternatively, a QTL on the right arm of chromosome III provides evidence of common genetic variation not present in the CB4856 strain that plays a role in the nematode zinc response. Because none of the known zinc-related genes are in this interval, this QTL might represent another novel gene that contributes to zinc resistance or sensitivity (**S6 File**). Our power to detect QTL would only improve with the phenotyping of more strains in the presence of high exogenous zinc.

## SQST-5 might function to negatively regulate other sequestosome-related genes

We show that strains with a functional copy of *sqst-5* are more sensitive to zinc than strains with a large deletion of the gene, indicating that *sqst-5* negatively regulates the zinc response. Using BLASTp (Wormbase.org, WS275), we searched for paralogs and identified five other members of the sequestosome-related family (*sqst-1, sqst-2, sqst-3, sqst-4,* and *C06G3.6*) each containing a ZZ-type domain, like *sqst-5*. Two of these genes have been previously implicated in the nematode stress response. The gene *sqst-1* is upregulated in response to hormetic heat shock [79]. Both SQST-1 and the human ortholog, SQSTM1/p62, have been shown to bind to and target ubiquitinated proteins to an organelle (sequestosome) for subsequent degradation by autophagy [79,80]. The ZZ-domain, particularly the zinc-coordinating Cys-X2-Cys residues, has been shown to be essential for this process [81,82]. Additionally, *sqst-3* is expressed in response to exogenous cadmium [83], suggesting that the sequestosome-related family might be involved

in divalent cation metal stress responses. If we connect these disparate results, then these genes could protect cells against zinc toxicity using sequestration and fusion with lysosomes. Alternatively, divalent cation metal stress could cause disruption of proteostasis and upregulation of sequestosome genes indirectly related to the specific metal stress. The role of this gene family in stress response has not been characterized using loss-of-function genetics, so we do not know whether the family is protective in response to exogenous stressors like zinc.

If the sequestosome-related genes do function to protect cells from high exogenous zinc, we would expect that loss-of-function of these genes should cause increased zinc sensitivity. However, loss-of-function of *sqst-5* caused increased zinc resistance, indicating that *sqst-5* might have a different function than other sequestosome-related genes. Although the exact function of SQST-5 is unknown, it is predicted to have protein kinase C and K63-linked polyubiquitin modification-dependent protein binding activity (Wormbase.org, WS275). From previous studies, we know that the ZZ-type domain is important for protein-protein interactions [66], and we discovered that the natural 111 bp deletion in the CB4856 strain causes a loss of this zinc-binding domain. It is possible that SQST-5 could function as an inhibitor of mechanisms that mitigate exogenous zinc, potentially by binding to other sequestesome-related proteins and inhibiting their activities. When SQST-5 is removed, the protein partner is no longer inhibited and is available to bind or capture the excess zinc in the environment, thus reducing the toxicity induced by high exogenous zinc. Biological processes that are finely balanced in homeostasis often contain both positive and negative regulators. Functional studies to directly test the role of *sqst-5* in the autophagy pathway, both in control conditions and in the presence of exogenous zinc, are necessary to provide insights into its function as a negative regulator of zinc homeostasis. Likewise, zinc responses of animals with targeted deletions of the other sequestosome-related genes are needed to fully define the roles for these genes in the *C. elegans* zinc response pathway. Overall, this study leverages natural genetic variation to discover a novel gene that

sensitizes nematodes to exogenous zinc, potentially by creating a negative feedback loop to regulate other sequestosome-related genes.

# Materials and methods

## Strains

Animals were grown at 20°C on modified nematode growth media (NGMA) containing 1% agar and 0.7% agarose to prevent burrowing and fed OP50 [44]. The two parental strains, the canonical laboratory strain, N2, and the wild isolate from Hawaii, CB4856, were used to generate all recombinant lines. 253 recombinant inbred advanced intercross lines (RIAILs) generated previously [34] (set 2 RIAILs) were used for zinc phenotyping and QTL mapping. A second set of 121 RIAILs generated previously [33] (set 1 RIAILs) were phenotyped for mediation analysis. All strains are listed in the Supplementary Material and are available upon request or from the *C. elegans* Natural Diversity Resource [32].

## Standard high-throughput fitness assay

For dose responses and RIAIL phenotyping, we used a high-throughput fitness assay (HTA) described previously [34]. In summary, populations of each strain were passaged and amplified on NGMA plates for four generations without starvation. In the fifth generation, gravid adults were bleach-synchronized and 25-50 embryos from each strain were aliquoted into 96-well microtiter plates at a final volume of 50 µL K medium [85]. The following day, arrested L1s were fed HB101 bacterial lysate (Pennsylvania State University Shared Fermentation Facility, State College, PA; [86]) at a final concentration of 5 mg/mL in K medium and were grown to the L4 larval stage for 48 hours at 20°C with constant shaking. Three L4 larvae were sorted into new 96-well microtiter plates containing 10 mg/mL HB101 bacterial lysate, 50 µM kanamycin, and either 1% water or zinc sulfate dissolved in 1% water using a large-particle flow cytometer (COPAS BIOSORT, Union

Biometrica; Holliston, MA). Sorted animals were grown for 96 hours at 20°C with constant shaking. The next generation of animals and the parents were treated with sodium azide (50 mM in 1X M9) to straighten their bodies for more accurate measurements. Animal length (TOF) and optical density (EXT) were quantified for every animal in each well using the COPAS BIOSORT and the medians of each well population (median.TOF and median.EXT) were used to estimate these traits. Animal length and optical density are both measures of nematode development; animals get longer and more optically dense (thicker and denser body composition) as they develop [34]. However, the COPAS BIOSORT measures optical density as a function of length. Because these two traits are highly correlated, we also generated a fourth trait (median.norm.EXT) which normalizes the optical density by length (EXT/TOF) in order to provide a means to compare optical densities regardless of animal lengths. Finally, brood size (norm.n) was calculated as the total number of animals in the well normalized by the number of parents originally sorted and provides an estimate of nematode reproductive fitness [34].

## Calculation of zinc-response traits

Phenotypic measurements collected by the BIOSORT were processed and analyzed using the R package *easysorter* [87] as described previously [35]. Briefly, raw data from the BIOSORT was read into R using the *read_data* function and contaminated wells were removed using the *remove_contamination* function. The *sumplate* function was used to calculate summary statistics per well and four main traits were output: median.TOF (animal length), median.EXT (animal optical density), median.norm.EXT (animal optical density normalized by animal length), and norm.n (brood size). When trait measurements were collected across multiple assay experiments, the *regress(assay = T)* function was used to fit the linear model *(phenotype ~ assay)* to account for variation among assays. Outliers were pruned using *prune_outliers* to remove wells beyond two standard deviations of the mean for highly replicated assays. Alternatively, for assays with low replication (dose response and RIAIL phenotyping), *bamf_prune* was used to remove wells

beyond two times the IQR plus the 75th quartile or two times the IQR minus the 25th quartile, unless at least 5% of the strains lie outside this range. Finally, zinc-specific effects were calculated using the *regress(assay = FALSE)* function, which subtracts the mean water (control) value from each zinc replicate for each strain using a linear model *(drug_phenotype ~ control_phenotype)*. The residual phenotypic values were used as the zinc-response phenotype for all downstream analyses. In this way, we addressed only the differences among strains that were caused by treatment with zinc and ignored minor phenotypic variation among strains in the control condition. Pairwise tests for statistically significant differences in the zinc response between strains were performed using the *TukeyHSD* function [88] on an ANOVA model with the formula *(phenotype ~ strain)*. For plotting purposes, these residual values were normalized from zero to one with zero being the well with the smallest value and one the well with the largest value.

## Zinc dose response

Four genetically divergent strains (N2, CB4856, JU258, and DL238) were treated with increasing concentrations of zinc using the standard high-throughput assay described above. A concentration of 500 µM zinc sulfate heptahydrate (Sigma #221376-100G) in water was selected for the linkage mapping experiments. This concentration provided a reproducible zinc-specific effect and maximizes between-strain variation and minimizes within-strain variation across the four traits. Broad-sense heritability was calculated from the dose response phenotypes using the *lmer* function in the *lme4* R package [89] with the formula *phenotype ~ 1 + (1 | strain)* for each dose.

## Linkage mapping

253 RIAILs (set 2 RIAILs) were phenotyped in both zinc and water using the standard high-throughput assay described above. Linkage mapping was performed for all four zinc-response

606 traits using the R package *linkagemapping* (https://github.com/AndersenLab/linkagemapping) as
607 described previously [35]. The cross object derived from the whole-genome sequencing of the
608 RIAILs containing 13,003 SNPs was loaded using the function
609 *load_cross_obj("N2xCB4856cross_full")*. The RIAIL phenotypes were merged into the cross
610 object using the *merge_pheno* function with the argument *set* = *2*. A forward search (*fsearch*
611 function) adapted from the *R/qtl* package [90] was used to calculate the logarithm of the odds
612 (LOD) scores for each genetic marker and each trait as $-n(ln(1-R^2)/2ln(10))$ where R is the
613 Pearson correlation coefficient between the RIAIL genotypes at the marker and trait phenotypes
614 [91]. A 5% genome-wide error rate was calculated by permuting the RIAIL phenotypes 1000
615 times. The marker with the highest LOD score above the significance threshold was selected as
616 the QTL then integrated into the model as a cofactor and mapping was repeated iteratively until
617 no further significant QTL were identified. Finally, the *annotate_lods* function was used to
618 calculate the effect size of each QTL and determine 95% confidence intervals defined by a 1.5
619 LOD drop from the peak marker using the argument *cutoff* = *chromosomal*. In the same manner,
620 linkage mapping was performed for three other divalent cation metals: 250 µM copper in water,
621 100 µM cadmium in water [43], and 350 µM nickel in water [75].
622
623 **Two-dimensional genome scan**
624 A two-dimensional genome scan to identify interacting loci was performed for animal optical
625 density (median.EXT) in zinc using the *scantwo* function from the *qtl* package [90] as described
626 previously [35,43]. Each pairwise combination of loci was tested for correlations with trait variation
627 in the RIAILs. A summary of the maximum interactive LOD score for each chromosome pair can
628 be output using the *summary* function. Significant interactions were identified by permuting the
629 phenotype data 1000 times and determining the 5% genome-wide error rate. The significant
630 interaction threshold for the zinc-response variation scantwo was 4.09.
631

## Construction of near-isogenic lines (NILs)

NILs were generated as previously described [35,41–43] by either backcrossing a selected RIAIL for six generations or *de novo* by crossing the parental strains N2 and CB4856 to create a heterozygous individual that is then backcrossed for six generations. PCR amplification of insertion-deletion (indel) variants between N2 and CB4856 were used to track the genomic interval. Smaller NILs to further break up the interval were created by backcrossing a NIL for one generation to create a heterozygous $F_1$ individual. The $F_1$ individuals were selfed, and the $F_2$ population was scored for recombination events. NILs were whole-genome sequenced to verify introgressions and the absence of other introgressed regions [35,43]. Reagents used to generate NILs and a summary of each introgression can be found in the **Supplemental Material**.

## Development of R Shiny application to visualize NIL phenotypes

An R shiny web app (version 1.4.0.2) was developed to visualize the results from the high-throughput assays and can be found here: https://katiesevans9.shinyapps.io/QTL_NIL/. To begin analysis, the user can find all data controls in a panel on the left-hand side of the screen. A test dataset is provided (user should check “Use sample data” checkbox) or the user can upload one of the supplementary files from the manuscript after downloading to their local computer. The user should select “water” as the control condition and “zinc” as the drug condition. In some cases, the user will need to choose a specific assay to view if multiple options are available. The user also has the option to view one of four drug-response traits (median.EXT, median.TOF, norm.n, and median.norm.EXT). Finally, the user should choose a chromosome to view, generally the chromosome which contains the highlighted QTL for that particular assay.

Along the top of the main panel, the user can navigate several tabs including “Control”, “Condition”, “Regressed”, “NIL Genotypes”, and “Help!”. The “Control”, “Condition”, and “Regressed” tabs each show the NIL genotypes along the selected chromosome (left) and the

NIL phenotypes for the selected trait (right) in the water condition (control), raw zinc condition (condition), or regressed zinc condition (regressed). The regressed data are shown in the manuscript. The user can hover their mouse above the NIL genotype or phenotype plots to see more information or zoom in on a specific area of the plot. Below this plot is an interactive datatable containing the pairwise strain comparisons for this condition and trait. The "NIL Genotypes" tab shows a plot of the NIL genotypes across all chromosomes, not just the chromosome selected by the user (top) and an interactive datatable with the genotypes of each strain across all chromosomes (bottom). The final tab, "Help!" provides the user with the instructions detailed here to help them use the Shiny App.

In addition to these basic controls, the user also has access to several advanced features. The user can choose a subset of strains to plot by checking the box labeled "Show a subset of strains?" and unchecking the boxes next to strains the user wishes to omit. Additionally, the user can plot the location of one or more QTL as a vertical line on the NIL genotype plot by checking the "Show QTL?" box. The user then chooses how many QTL to show and uses the appropriate slider input below to designate the genomic positions of each QTL. Finally, if the "Show genotype?" box is checked, the genotype of each strain at each QTL position will be shown on the phenotype plot as an orange "N" representing N2 and a blue "C" representing CB4856.

## Mediation analysis

121 RIAILs (set 1 RIAILs) were phenotyped in both zinc and water using the standard high-throughput assay described above. Microarray expression for 14,107 probes were previously collected from the set 1 RIAILs [50], filtered [44], and mapped using linkage mapping with 13,003 SNPs [63]. Mediation scores were calculated with bootstrapping using the *mediation* R package [92] as previously described [63] for each of the 19 probes (including *ver-2/sqst-5*, A_12_P104472) with an eQTL on the left arm of chromosome III. Briefly, a mediator model *(expression ~ genotype)* and an outcome model *(phenotype ~ expression + genotype)* were used

683 to calculate the proportion of the QTL effect that can be explained by variation in gene expression.
684 All expression and eQTL data can be found at
685 https://github.com/AndersenLab/scb1_mediation_manuscript.
686

687 **Generation of deletion strains**

688 Deletion alleles for *sqst-5* and *ver-2* were generated as previously described using CRISPR-Cas9
689 genome editing [35,93]. Briefly, 5' and 3' guide RNAs were designed with the highest possible on-
690 target and off-target scores [94] and ordered from Synthego (Redwood City, CA). The following
691 CRISPR injection mix was assembled and incubated for an hour before injection: 1 µM *dpy-10*
692 sgRNA, 5 µM of each sgRNA for the gene of interest, 0.5 µM of a single-stranded
693 oligodeoxynucleotide template for homology-directed repair of *dpy-10* (IDT, Skokie, IL), and 5 µM
694 Cas9 protein (Q3B Berkeley, Berkeley, CA) in water. Young adults were mounted onto agar
695 injection pads, injected in either the anterior or posterior arm of the gonad, and allowed to recover
696 on 6 cm plates. After 12 hours, survivors were transferred to individual 6 cm plates and allowed
697 to lay embryos. Two days later, the F1 progeny were screened and individuals with Rol or Dpy
698 phenotypes were selected and transferred clonally to new 6 cm plates. After 48 hours, the F1
699 individuals were genotyped by PCR flanking the desired deletions. Individuals with heterozygous
700 or homozygous deletions were propagated and genotyped for at least two additional generations
701 to ensure homozygosity and to cross out the Rol mutation. Deletion amplicons were Sanger
702 sequenced to identify the exact location of the deletion. This information as well as all reagents
703 used to generate deletion alleles are detailed in the **Supplemental Material**.
704

705 **Modified high-throughput fitness assay**

706 Dominance and validation of candidate genes were tested using a modified version of the
707 standard high-throughput assay detailed above as previously described [35,63]. For candidate

gene testing, strains were propagated for two generations, bleach-synchronized in six independent replicates, and titered at a concentration of 25-50 embryos per well of a 96-well microtiter plate. For dominance and hemizygosity assays, strains (males and hermaphrodites) were propagated and amplified for two generations. For each cross, 30 hermaphrodites and 60 males were placed onto each of four 6 cm plates and allowed to mate for 48 hours. Mated hermaphrodites were transferred to a clean 6 cm plate and allowed to lay embryos for eight hours. After the egg-laying period, adults were manually removed and embryos were collected by vigorous washing with 1X M9. Embryos were resuspended in K medium and titered to a concentration of 25 embryos per well of a 96-well microtiter plate. For both assays, arrested L1s were fed HB101 bacterial lysate the following day at a final concentration of 5 mg/mL with either water or zinc. After 48 hours of growth at 20°C with constant shaking, nematodes were treated with sodium azide (5 mM in water) prior to analysis of animal length and optical density using the COPAS BIOSORT. Because only one generation of growth was observed, brood size was not calculated. Lower drug concentrations were needed to see the previous effect because of the modified timing of the drug delivery. A concentration of 250 μM zinc in water was used for these experiments.

## Local alignment of the *sqst-5* region using long-read sequence data

To confirm the putative *sqst-5* deletion in CB4856, we aligned the long-read assembly for CB4856 [65] to the N2 reference genome using NUCmer (version v3.1) [95]. Using this alignment, we identified the coordinates of *sqst-5* in CB4856 and extracted the sequence using BEDtools (version v2.29.2) [96]. We aligned the unspliced N2 *sqst-5* transcript sequence (WormBase WS273) and the N2 SQST-5 protein sequence to this extracted CB4856 sequence using Clustal Omega [97] and GeneWise [98], respectively. Gene prediction in CB4856 was run using Augustus [99]. We visually inspected both alignments to identify the length of the deletion in CB4856 and identify the effect of the deletion of the CB4856 SQST-5 protein sequence.

734

735 **Assessment of strain relatedness through neighbor-joining tree**

736 Variant data for dendrogram comparisons were assembled by constructing a FASTA file with the
737 genome-wide variant positions across all strains and subsetting to keep only variants near *sqst-*
738 *5* (III:145917-148620). Genotype data were acquired from the latest VCF release (release
739 20180517) from CeNDR. Multiple sequence comparison by log-expectation (MUSCLE, version
740 v3.8.31) [100] was used to generate neighbor-joining trees. A second neighbor-joining tree was
741 constructed with all the variants within the QTL confidence interval for comparison (III:4664-
742 597553). Both trees were identical.

743

744 **Genome wide association mapping**

745 Eighty-one wild isolates were phenotyped in both zinc and water using the standard high-
746 throughput assay described above. Genome-wide association (GWA) mappings were performed
747 for all four traits using the R package *cegwas2* (https://github.com/AndersenLab/cegwas2-nf) as
748 described previously [41]. Genotype data were acquired from the latest VCF release (release
749 20180517) from CeNDR. We used BCFtools [101] to filter variants with missing genotypes and
750 variants below a 5% minor allele frequency. We used PLINK v1.9 [102,103] to LD-prune
751 genotypes. The additive kinship matrix was generated from the 64,046 markers using the *A.mat*
752 function in the *rrBLUP* R package [104]. Because these markers have high LD, we performed
753 eigen decomposition of the correlation matrix of the genotype matrix to identify 477 independent
754 tests [41]. We used the *GWAS* function from the *rrBLUP* package to perform genome-wide
755 mapping. Significance was determined in two ways: a strict Bonferroni threshold and a more
756 lenient eigenvalue threshold set by the number of independent tests in the genotype matrix.
757 Confidence intervals were defined as +/- 150 SNVs from the rightmost and leftmost markers that
758 passed the significance threshold.

759

760 **Statistical analysis**

761 All statistical tests of phenotypic differences between strains were performed using the *TukeyHSD*
762 function [88] on an ANOVA model with the formula *(phenotype ~ strain)*. The *p-values* for
763 individual pairwise strain comparisons were adjusted for multiple comparisons (Bonferroni). The
764 datasets and code for generating figures can be found at
765 https://github.com/AndersenLab/zinc_manuscript.

766

767 ## Acknowledgements

768 We would like to thank Bryn Gaertner, Samuel Rosenberg, and Tyler Shimko, for assistance with
769 mapping zinc sensitivities and members of the Andersen Lab for helpful comments on the
770 manuscript. Additionally, we would like to thank WormBase and the *C. elegans* Natural Diversity
771 Resource (CeNDR) for data critical for our analysis.

772

773 ## References

774 1. Rosen BP. Metals in biology: past, present, and future. In: Tamas MJ, Martinoia E, editors.
775 Molecular Biology of Metal Homeostasis and Detoxification: From Microbes to Man. Berlin,
776 Heidelberg: Springer Berlin Heidelberg; 2006. pp. 485–505.

777 2. Oleszkiewicz JA, Sharma VK. Stimulation and inhibition of anaerobic processes by heavy
778 metals—A review. Biological Wastes. 1990;31: 45–67.

779 3. Vallee BL, Falchuk KH. The biochemical basis of zinc physiology. Physiol Rev. 1993;73:
780 79–118.

781 4. Frederickson CJ, Bush AI. Synaptically released zinc: physiological functions and

pathological effects. Biometals. 2001;14: 353–366.

5. Colvin RA, Fontaine CP, Laskowski M, Thomas D. Zn2+ transporters and Zn2+ homeostasis in neurons. Eur J Pharmacol. 2003;479: 171–185.

6. Wall MJ. A role for zinc in cerebellar synaptic transmission? Cerebellum. 2005;4: 224–229.

7. Yamasaki S, Sakata-Sogawa K, Hasegawa A, Suzuki T, Kabu K, Sato E, et al. Zinc is a novel intracellular second messenger. J Cell Biol. 2007;177: 637–645.

8. Dietrich N, Tan C-H, Cubillas C, Earley BJ, Kornfeld K. Insights into zinc and cadmium biology in the nematode Caenorhabditis elegans. Arch Biochem Biophys. 2016;611: 120–133.

9. Yoder JH, Chong H, Guan K-I, Han M. Modulation of KSR activity in Caenorhabditis elegans by Zn ions, PAR-1 kinase and PP2A phosphatase. EMBO J. 2004;23: 111–119.

10. Bruinsma JJ, Jirakulaporn T, Muslin AJ, Kornfeld K. Zinc ions and cation diffusion facilitator proteins regulate Ras-mediated signaling. Dev Cell. 2002;2: 567–578.

11. Samet JM, Dewar BJ, Wu W, Graves LM. Mechanisms of Zn(2+)-induced signal initiation through the epidermal growth factor receptor. Toxicol Appl Pharmacol. 2003;191: 86–93.

12. Wu W, Graves LM, Jaspers I, Devlin RB, Reed W, Samet JM. Activation of the EGF receptor signaling pathway in human airway epithelial cells exposed to metals. Am J Physiol. 1999;277: L924–31.

13. Roohani N, Hurrell R, Kelishadi R, Schulin R. Zinc and its importance for human health: An integrative review. J Res Med Sci. 2013;18: 144–157.

14. Fernandes G, Nair M, Onoe K, Tanaka T, Floyd R, Good RA. Impairment of cell-mediated

immunity functions by dietary zinc deficiency in mice. Proc Natl Acad Sci U S A. 1979;76: 457–461.

15. Zhao X-Q, Bai F-W. Zinc and yeast stress tolerance: micronutrient plays a big role. J Biotechnol. 2012;158: 176–183.

16. Navarro JA, Schneuwly S. Copper and Zinc Homeostasis: Lessons from Drosophila melanogaster. Front Genet. 2017;8: 223.

17. Fosmire GJ. Zinc toxicity. Am J Clin Nutr. 1990;51: 225–227.

18. Warnhoff K, Roh HC, Kocsisova Z, Tan C-H, Morrison A, Croswell D, et al. The Nuclear Receptor HIZR-1 Uses Zinc as a Ligand to Mediate Homeostasis in Response to High Zinc. PLoS Biol. 2017;15: e2000094.

19. Zhao Y, Tan C-H, Krauchunas A, Scharf A, Dietrich N, Warnhoff K, et al. The zinc transporter ZIPT-7.1 regulates sperm activation in nematodes. PLoS Biol. 2018;16: e2005069.

20. Dietrich N, Schneider DL, Kornfeld K. A pathway for low zinc homeostasis that is conserved in animals and acts in parallel to the pathway for high zinc homeostasis. Nucleic Acids Res. 2017;45: 11658–11672.

21. Davis DE, Roh HC, Deshmukh K, Bruinsma JJ, Schneider DL, Guthrie J, et al. The cation diffusion facilitator gene cdf-2 mediates zinc metabolism in Caenorhabditis elegans. Genetics. 2009;182: 1015–1033.

22. Andreini C, Banci L, Bertini I, Rosato A. Zinc through the three domains of life. J Proteome Res. 2006;5: 3173–3178.

23. Bruinsma JJ, Schneider DL, Davis DE, Kornfeld K. Identification of mutations in

825 Caenorhabditis elegans that cause resistance to high levels of dietary zinc and analysis
826 using a genomewide map of single nucleotide polymorphisms scored by pyrosequencing.
827 Genetics. 2008;179: 811–828.

828 24. Murphy JT, Bruinsma JJ, Schneider DL, Collier S, Guthrie J, Chinwalla A, et al. Histidine
829 protects against zinc and nickel toxicity in Caenorhabditis elegans. PLoS Genet. 2011;7:
830 e1002013.

831 25. Warnhoff K, Murphy JT, Kumar S, Schneider DL, Peterson M, Hsu S, et al. The DAF-16
832 FOXO transcription factor regulates natc-1 to modulate stress resistance in Caenorhabditis
833 elegans, linking insulin/IGF-1 signaling to protein N-terminal acetylation. PLoS Genet.
834 2014;10: e1004703.

835 26. Wang Y, Ezemaduka AN. Combined effect of temperature and zinc on Caenorhabditis
836 elegans wild type and daf-21 mutant strains. J Therm Biol. 2014;41: 16–20.

837 27. Roh HC, Collier S, Deshmukh K, Guthrie J, Robertson JD, Kornfeld K. ttm-1 encodes CDF
838 transporters that excrete zinc from intestinal cells of C. elegans and act in a parallel
839 negative feedback circuit that promotes homeostasis. PLoS Genet. 2013;9: e1003522.

840 28. Roh HC, Collier S, Guthrie J, Robertson JD, Kornfeld K. Lysosome-related organelles in
841 intestinal cells are a zinc storage site in C. elegans. Cell Metab. 2012;15: 88–99.

842 29. Sterken MG, Snoek LB, Kammenga JE, Andersen EC. The laboratory domestication of
843 Caenorhabditis elegans. Trends Genet. 2015;31: 224–231.

844 30. Crombie TA, Zdraljevic S, Cook DE, Tanny RE, Brady SC, Wang Y, et al. Deep sampling of
845 Hawaiian Caenorhabditis elegans reveals high genetic diversity and admixture with global
846 populations. Elife. 2019;8: e50465.

847 31. Andersen EC, Gerke JP, Shapiro JA, Crissman JR, Ghosh R, Bloom JS, et al.
848 Chromosome-scale selective sweeps shape Caenorhabditis elegans genomic diversity. Nat
849 Genet. 2012;44: 285–290.

850 32. Cook DE, Zdraljevic S, Roberts JP, Andersen EC. CeNDR, the Caenorhabditis elegans
851 natural diversity resource. Nucleic Acids Res. 2016. doi:10.1093/nar/gkw893

852 33. Rockman MV, Kruglyak L. Recombinational landscape and population genomics of
853 Caenorhabditis elegans. PLoS Genet. 2009;5: e1000419.

854 34. Andersen EC, Shimko TC, Crissman JR, Ghosh R, Bloom JS, Seidel HS, et al. A Powerful
855 New Quantitative Genetics Platform, Combining Caenorhabditis elegans High-Throughput
856 Fitness Assays with a Large Collection of Recombinant Strains. G3 . 2015;5: 911–920.

857 35. Brady SC, Zdraljevic S, Bisaga KW, Tanny RE, Cook DE, Lee D, et al. A Novel Gene
858 Underlies Bleomycin-Response Variation in Caenorhabditis elegans. Genetics. 2019;212:
859 1453–1468.

860 36. Thompson OA, Snoek LB, Nijveen H, Sterken MG, Volkers RJM, Brenchley R, et al.
861 Remarkably Divergent Regions Punctuate the Genome Assembly of the Caenorhabditis
862 elegans Hawaiian Strain CB4856. Genetics. 2015;200: 975–989.

863 37. McGrath PT, Rockman MV, Zimmer M, Jang H, Macosko EZ, Kruglyak L, et al. Quantitative
864 mapping of a digenic behavioral trait implicates globin variation in C. elegans sensory
865 behaviors. Neuron. 2009;61: 692–699.

866 38. Bendesky A, Bargmann CI. Genetic contributions to behavioural diversity at the gene-
867 environment interface. Nat Rev Genet. 2011;12: 809–820.

868 39. Lee D, Yang H, Kim J, Brady S, Zdraljevic S, Zamanian M, et al. The genetic basis of

natural variation in a phoretic behavior. Nat Commun. 2017;8: 273.

40. Singh KD, Roschitzki B, Snoek LB, Grossmann J, Zheng X, Elvin M, et al. Natural Genetic Variation Influences Protein Abundances in C. elegans Developmental Signalling Pathways. PLoS One. 2016;11: e0149418.

41. Zdraljevic S, Fox BW, Strand C, Panda O, Tenjo FJ, Brady SC, et al. Natural variation in C. elegans arsenic toxicity is explained by differences in branched chain amino acid metabolism. Elife. 2019;8. doi:10.7554/eLife.40260

42. Zdraljevic S, Strand C, Seidel HS, Cook DE, Doench JG, Andersen EC. Natural variation in a single amino acid substitution underlies physiological responses to topoisomerase II poisons. PLoS Genet. 2017;13: e1006891.

43. Evans KS, Brady SC, Bloom JS, Tanny RE, Cook DE, Giuliani SE, et al. Shared Genomic Regions Underlie Natural Variation in Diverse Toxin Responses. Genetics. 2018. doi:10.1534/genetics.118.301311

44. Andersen EC, Bloom JS, Gerke JP, Kruglyak L. A variant in the neuropeptide receptor npr-1 is a major determinant of Caenorhabditis elegans growth and physiology. PLoS Genet. 2014;10: e1004156.

45. Viñuela A, Snoek LB, Riksen JAG, Kammenga JE. Genome-wide gene expression regulation as a function of genotype and age in C. elegans. Genome Res. 2010;20: 929–937.

46. Doroszuk A, Snoek LB, Fradin E, Riksen J, Kammenga J. A genome-wide library of CB4856/N2 introgression lines of Caenorhabditis elegans. Nucleic Acids Res. 2009;37: e110.

47. Snoek LB, Orbidans HE, Stastna JJ, Aartse A, Rodriguez M, Riksen JAG, et al. Widespread genomic incompatibilities in Caenorhabditis elegans. G3 . 2014;4: 1813–1823.

48. Rodriguez M, Snoek LB, Riksen JAG, Bevers RP, Kammenga JE. Genetic variation for stress-response hormesis in C. elegans lifespan. Exp Gerontol. 2012;47: 581–587.

49. Glater EE, Rockman MV, Bargmann CI. Multigenic natural variation underlies Caenorhabditis elegans olfactory preference for the bacterial pathogen Serratia marcescens. G3 . 2014;4: 265–276.

50. Rockman MV, Skrovanek SS, Kruglyak L. Selection at linked sites shapes heritable phenotypic variation in C. elegans. Science. 2010;330: 372–376.

51. Zamanian M, Cook DE, Zdraljevic S, Brady SC, Lee D, Lee J, et al. Discovery of genomic intervals that underlie nematode responses to benzimidazoles. PLoS Negl Trop Dis. 2018;12: e0006368.

52. Bendesky A, Tsunozaki M, Rockman MV, Kruglyak L, Bargmann CI. Catecholamine receptor polymorphisms affect decision-making in C. elegans. Nature. 2011;472: 313–318.

53. Bendesky A, Pitts J, Rockman MV, Chen WC, Tan M-W, Kruglyak L, et al. Long-range regulatory polymorphisms affecting a GABA receptor constitute a quantitative trait locus (QTL) for social behavior in Caenorhabditis elegans. PLoS Genet. 2012;8: e1003157.

54. Schmid T, Snoek LB, Fröhli E, van der Bent ML, Kammenga J, Hajnal A. Systemic Regulation of RAS/MAPK Signaling by the Serotonin Metabolite 5-HIAA. PLoS Genet. 2015;11: e1005236.

55. Balla KM, Andersen EC, Kruglyak L, Troemel ER. A wild C. elegans strain has enhanced epithelial immunity to a natural microsporidian parasite. PLoS Pathog. 2015;11: e1004583.

913 56. Kammenga JE, Doroszuk A, Riksen JAG, Hazendonk E, Spiridon L, Petrescu A-J, et al. A
914 Caenorhabditis elegans wild type defies the temperature-size rule owing to a single
915 nucleotide polymorphism in tra-3. PLoS Genet. 2007;3: e34.

916 57. Gutteling EW, Riksen JAG, Bakker J, Kammenga JE. Mapping phenotypic plasticity and
917 genotype-environment interactions affecting life-history traits in Caenorhabditis elegans.
918 Heredity . 2007;98: 28–37.

919 58. Gutteling EW, Doroszuk A, Riksen JAG, Prokop Z, Reszka J, Kammenga JE.
920 Environmental influence on the genetic correlations between life-history traits in
921 Caenorhabditis elegans. Heredity . 2007;98: 206–213.

922 59. Li Y, Alvarez OA, Gutteling EW, Tijsterman M, Fu J, Riksen JAG, et al. Mapping
923 determinants of gene expression plasticity by genetical genomics in C. elegans. PLoS
924 Genet. 2006;2: e222.

925 60. Reddy KC, Andersen EC, Kruglyak L, Kim DH. A polymorphism in npr-1 is a behavioral
926 determinant of pathogen susceptibility in C. elegans. Science. 2009;323: 382–384.

927 61. Seidel HS, Ailion M, Li J, van Oudenaarden A, Rockman MV, Kruglyak L. A novel sperm-
928 delivered toxin causes late-stage embryo lethality and transmission ratio distortion in C.
929 elegans. PLoS Biol. 2011;9: e1001115.

930 62. Seidel HS, Rockman MV, Kruglyak L. Widespread genetic incompatibility in C. elegans
931 maintained by balancing selection. Science. 2008;319: 589–594.

932 63. Evans KS, Andersen EC. The Gene scb-1 Underlies Variation in Caenorhabditis elegans
933 Chemotherapeutic Responses. G3 . 2020. doi:10.1534/g3.120.401310

934 64. Dittrich-Reed DR, Fitzpatrick BM. Transgressive Hybrids as Hopeful Monsters. Evol Biol.

2013;40: 310–315.

65. Kim C, Kim J, Kim S, Cook DE, Evans KS, Andersen EC, et al. Long-read sequencing reveals intra-species tolerance of substantial structural variations and new subtelomere formation in C. elegans. Genome Res. 2019;29: 1023–1035.

66. Ponting CP, Blake DJ, Davies KE, Kendrick-Jones J, Winder SJ. ZZ and TAZ: new putative zinc fingers in dystrophin and other proteins. Trends Biochem Sci. 1996;21: 11–13.

67. Legge GB, Martinez-Yamout MA, Hambly DM, Trinh T, Lee BM, Dyson HJ, et al. ZZ domain of CBP: an unusual zinc finger fold in a protein interaction module. J Mol Biol. 2004;343: 1081–1093.

68. Green JWM, Snoek LB, Kammenga JE, Harvey SC. Genetic mapping of variation in dauer larvae development in growing populations of Caenorhabditis elegans. Heredity . 2013;111: 306–313.

69. Mackay TFC. Epistasis and quantitative traits: using model organisms to study gene-gene interactions. Nat Rev Genet. 2014;15: 22–33.

70. Metzger BPH, Wittkopp PJ. Compensatory trans-regulatory alleles minimizing variation in TDH3 expression are common within Saccharomyces cerevisiae. Evol Lett. 2019;3: 448–461.

71. Gaertner BE, Parmenter MD, Rockman MV, Kruglyak L, Phillips PC. More than the sum of its parts: a complex epistatic network underlies natural variation in thermal preference behavior in Caenorhabditis elegans. Genetics. 2012;192: 1533–1542.

72. Shao H, Burrage LC, Sinasac DS, Hill AE, Ernest SR, O'Brien W, et al. Genetic architecture of complex traits: large phenotypic effects and pervasive epistasis. Proc Natl Acad Sci U S

A. 2008;105: 19910–19914.

73. Kroymann J, Mitchell-Olds T. Epistasis and balanced polymorphism influencing complex trait variation. Nature. 2005;435: 95–98.

74. Steinmetz LM, Sinha H, Richards DR, Spiegelman JI, Oefner PJ, McCusker JH, et al. Dissecting the architecture of a quantitative trait locus in yeast. Nature. 2002;416: 326–330.

75. Bernstein MR, Zdraljevic S, Andersen EC, Rockman MV. Tightly linked antagonistic-effect loci underlie polygenic phenotypic variation in C. elegans. Evol Lett. 2019;3: 462–473.

76. Mackay TFC, Stone EA, Ayroles JF. The genetics of quantitative traits: challenges and prospects. Nat Rev Genet. 2009;10: 565–577.

77. Rockman MV. The QTN program and the alleles that matter for evolution: all that's gold does not glitter. Evolution. 2012;66: 1–17.

78. Boyle EA, Li YI, Pritchard JK. An Expanded View of Complex Traits: From Polygenic to Omnigenic. Cell. 2017;169: 1177–1186.

79. Kumsta C, Chang JT, Lee R, Tan EP, Yang Y, Loureiro R, et al. The autophagy receptor p62/SQST-1 promotes proteostasis and longevity in C. elegans by inducing autophagy. Nat Commun. 2019;10: 5648.

80. Gatica D, Lahiri V, Klionsky DJ. Cargo recognition and degradation by selective autophagy. Nat Cell Biol. 2018;20: 233–242.

81. Zhang Y, Mi W, Xue Y, Shi X, Kutateladze TG. The ZZ domain as a new epigenetic reader and a degradation signal sensor. Crit Rev Biochem Mol Biol. 2019;54: 1–10.

82. Cha-Molstad H, Yu JE, Feng Z, Lee SH, Kim JG, Yang P, et al.

978 p62/SQSTM1/Sequestosome-1 is an N-recognin of the N-end rule pathway which
979 modulates autophagosome biogenesis. Nat Commun. 2017;8: 102.

980 83. Cui Y, McBride SJ, Boyd WA, Alper S, Freedman JH. Toxicogenomic analysis of
981 Caenorhabditis elegans reveals novel genes and pathways involved in the resistance to
982 cadmium toxicity. Genome Biol. 2007;8: R122.

983 84. Ghosh R, Andersen EC, Shapiro JA, Gerke JP, Kruglyak L. Natural variation in a chloride
984 channel subunit confers avermectin resistance in C. elegans. Science. 2012;335: 574–578.

985 85. Boyd WA, Smith MV, Freedman JH. Caenorhabditis elegans as a model in developmental
986 toxicology. Methods Mol Biol. 2012;889: 15–24.

987 86. García-González AP, Ritter AD, Shrestha S, Andersen EC, Yilmaz LS, Walhout AJM.
988 Bacterial Metabolism Affects the C. elegans Response to Cancer Chemotherapeutics. Cell.
989 2017;169: 431–441.e8.

990 87. Shimko TC, Andersen EC. COPASutils: an R package for reading, processing, and
991 visualizing data from COPAS large-particle flow cytometers. PLoS One. 2014;9: e111090.

992 88. R Core Team. R: A Language and Environment for Statistical Computing. Vienna, Austria:
993 R Foundation for Statistical Computing; 2017. Available: https://www.R-project.org/

994 89. Bates D, Mächler M, Bolker B, Walker S. Fitting Linear Mixed-Effects Models Using lme4.
995 Journal of Statistical Software, Articles. 2015;67: 1–48.

996 90. Broman KW, Wu H, Sen S, Churchill GA. R/qtl: QTL mapping in experimental crosses.
997 Bioinformatics. 2003;19: 889–890.

998 91. Bloom JS, Ehrenreich IM, Loo WT, Lite T-LV, Kruglyak L. Finding the sources of missing
999 heritability in a yeast cross. Nature. 2013;494: 234–237.

1000 92. Tingley D, Yamamoto T, Hirose K, Keele L, Imai K. mediation: R Package for Causal
1001 Mediation Analysis. Journal of Statistical Software, Articles. 2014;59: 1–38.

1002 93. Hahnel SR, Zdraljevic S, Rodriguez BC, Zhao Y, McGrath PT, Andersen EC. Extreme
1003 allelic heterogeneity at a Caenorhabditis elegans beta-tubulin locus explains natural
1004 resistance to benzimidazoles. PLoS Pathog. 2018;14: e1007226.

1005 94. Doench JG, Fusi N, Sullender M, Hegde M, Vaimberg EW, Donovan KF, et al. Optimized
1006 sgRNA design to maximize activity and minimize off-target effects of CRISPR-Cas9. Nat
1007 Biotechnol. 2016;34: 184–191.

1008 95. Kurtz S, Phillippy A, Delcher AL, Smoot M, Shumway M, Antonescu C, et al. Versatile and
1009 open software for comparing large genomes. Genome Biol. 2004;5: R12.

1010 96. Quinlan AR, Hall IM. BEDTools: a flexible suite of utilities for comparing genomic features.
1011 Bioinformatics. 2010;26: 841–842.

1012 97. Sievers F, Wilm A, Dineen D, Gibson TJ, Karplus K, Li W, et al. Fast, scalable generation of
1013 high-quality protein multiple sequence alignments using Clustal Omega. Mol Syst Biol.
1014 2011;7: 539.

1015 98. Birney E, Clamp M, Durbin R. GeneWise and Genomewise. Genome Res. 2004;14: 988–
1016 995.

1017 99. Stanke M, Morgenstern B. AUGUSTUS: a web server for gene prediction in eukaryotes that
1018 allows user-defined constraints. Nucleic Acids Res. 2005;33: W465–7.

1019 100. Edgar RC. MUSCLE: multiple sequence alignment with high accuracy and high
1020 throughput. Nucleic Acids Res. 2004;32: 1792–1797.

1021 101. Li H. A statistical framework for SNP calling, mutation discovery, association mapping

and population genetical parameter estimation from sequencing data. Bioinformatics. 2011;27: 2987–2993.

102. Purcell S, Neale B, Todd-Brown K, Thomas L, Ferreira MAR, Bender D, et al. PLINK: a tool set for whole-genome association and population-based linkage analyses. Am J Hum Genet. 2007;81: 559–575.

103. Chang CC, Chow CC, Tellier LC, Vattikuti S, Purcell SM, Lee JJ. Second-generation PLINK: rising to the challenge of larger and richer datasets. Gigascience. 2015;4: 7.

104. Endelman JB. Ridge Regression and Other Kernels for Genomic Selection with R Package rrBLUP. Plant Genome. 2011;4: 250–255.

## Supporting information captions

**S1 Fig. Dose response with four divergent wild isolates.** Results from the zinc dose response HTA for brood size (norm.n), animal length (median.TOF), animal optical density (median.EXT), and normalized optical density (median.norm.EXT). For each trait, drug concentration (μM) (x-axis) is plotted against phenotype subtracted from control (y-axis), colored by strain (CB4856: blue, DL238: green, JU258: purple, N2: orange). A red asterisk indicates the dose selected for linkage mapping analysis.

**S2 Fig. Linkage mapping identifies 12 QTL across three traits in response to high zinc. A)** Normalized residual phenotype (y-axis) of 253 RIAILs (x-axis) in response to zinc supplementation. The parental strains are colored: N2, orange; CB4856, blue. **B)** Linkage mapping results are shown. Genomic position (x-axis) is plotted against the logarithm of the odds (LOD) score (y-axis) for 13,003 genomic markers. Each significant QTL is indicated by a red triangle at the peak marker, and a blue rectangle shows the 95% confidence interval around the peak marker. The percentage of the total variance in the RIAIL population that can be explained by each QTL is shown above the QTL. **C)** For each QTL, the normalized residual phenotype (y-

axis) of RIAILs split by genotype at the marker with the maximum LOD score (x-axis) are plotted as Tukey box plots. Each point corresponds to a unique recombinant strain. Strains with the N2 allele are colored orange and strains with the CB4856 allele are colored blue.

**S3 Fig. Two dimensional genome scan for median optical density (median.EXT) in zinc.** Log of the odds (LOD) scores are shown for each pairwise combination of loci, split by chromosome. The upper-left triangle contains the epistasis LOD scores and the lower-right triangle contains the LOD scores for the full model. LOD scores are colored, increasing from purple to green to yellow. The LOD scores for the epistasis model are shown on the left of the color scale and the LOD scores for the full model are shown on the right.

**S4 Fig. Reaction norm shows additive QTL effects between chromosome III and V.** Normalized residual median optical density in zinc (median.EXT, y-axis) of RIAILs split by genotype at the chromosome III QTL (x-axis) are plotted as the mean of the population +/- the standard deviation, colored by the genotype at the chromosome V QTL.

**S5 Fig. Validating QTL using near-isogenic lines (NILs). A)** Strain genotypes are shown as colored rectangles (N2: orange, CB4856: blue) in detail for each chromosome (left) and in general for the rest of the chromosomes (right). The solid vertical line represents the peak marker of the QTL and the dashed vertical lines represent the confidence interval. **B)** Normalized residual median optical density in zinc (median.EXT, x-axis) is plotted as Tukey box plots against strain (y-axis). The parental strains N2 and CB4856 are colored orange and blue, respectively. NILs are colored grey. Statistical significance of each strain compared to its parental strain (ECA838, ECA240, ECA232, ECA931, and ECA929 to N2 and ECA859, ECA241, ECA230, and ECA828 to CB4856) is shown above each strain and colored by the parent strain it was tested against (ns = non-significant (p-value > 0.05); *, **, ***, and *** = significant (p-value < 0.05, 0.01, 0.001, or 0.0001, respectively).

**S6 Fig. Dose response for modified HTA.** Results from the zinc dose response with the modified HTA for median optical density (median.EXT). Drug concentration (μM) (x-axis) is plotted

against phenotype subtracted from control (y-axis), colored by strain (CB4856: blue, N2: orange). A red asterisk indicates the dose selected for further analysis.

**S7 Fig. The gene *sqst-5*, not *ver-2*, has an eQTL.** Original gene model for *ver-2* is shown with colored boxes representing exons connected by lines representing introns. Exons are colored blue for the new gene model for *ver-2* and purple for *sqst-5*. The black rectangles below represent approximate locations of CRISPR-mediated deletions of *ver-2* or *sqst-5*. The location of the microarray probe is designated as a red rectangle below the plot.

**S8 Fig. Testing the role of *sqst-5* in the zinc response. A)** Strain genotypes are shown as colored rectangles (N2: orange, CB4856: blue) in detail for chromosome III (left) and in general for the rest of the chromosomes (right). The dashed vertical line represents the location of *sqst-5* and grey triangles represent *sqst-5* deletions. **B)** Normalized residual median optical density in zinc (median.EXT, x-axis) is plotted as Tukey box plots against strain (y-axis). Statistical significance of each strain compared to its parental strain (ECA838, ECA1377, and ECA1378 to N2 and ECA859, ECA1379, and ECA1380 to CB4856) is shown above each strain and colored by the parent strain it was tested against (ns = non-significant (p-value > 0.05); *, **, ***, and *** = significant (p-value < 0.05, 0.01, 0.001, or 0.0001, respectively).

**S9 Fig. Isolating the effect of *sqst-5* in the zinc response. A)** Strain genotypes are shown as colored rectangles (N2: orange, CB4856: blue) in detail for chromosome III (left) and in general for the rest of the chromosomes (right). The dashed vertical line represents the location of *sqst-5* and grey triangles represent *sqst-5* deletions. **B)** Normalized residual median optical density in zinc (median.EXT, x-axis) is plotted as Tukey box plots against strain (y-axis). The N2 strain, which is usually resistant to zinc, was sick in this experiment. Statistical significance of each strain compared to ECA859 is shown above each strain (ns = non-significant (p-value > 0.05); *, **, ***, and *** = significant (p-value < 0.05, 0.01, 0.001, or 0.0001, respectively).

**S10 Fig. Geographical distribution of 328 wild isolates.** Map of wild isolates. Strains are colored by the variation haplotype at sqst-5 (Wild-type: grey, N2: orange, CB4856: navy, Deletion:

magenta, Other putative structural variation: light pink). Strains with the deletion are labeled.

**S11 Fig. Genome-wide association (GWA) mapping identifies eight QTL across four traits in response to high zinc. A)** Normalized residual phenotype (y-axis) of 81 wild isolates (x-axis) in response to zinc supplementation. Strains are colored by the parental strains N2 (orange) and CB4856 (blue) or by the *sqst-5* variation (Deletion: magenta, other variation: light pink) **B)** GWA results are shown. Genomic position (x-axis) is plotted against the *-log10(p)* value (y-axis) for each SNV. SNVs are colored pink if they pass the genome-wide eigen-decomposition significance threshold designated by the dotted grey line. The solid grey line represents the more stringent Bonferroni significance threshold. The genomic regions of interest that pass the significance threshold are highlighted by blue rectangles. **C)** For each QTL, the normalized residual phenotype (y-axis) of strains split by genotype at the peak marker (x-axis) are plotted as Tukey box plots. Each point corresponds to a wild isolate strain. Strains with the N2 reference allele are colored grey, and strains with an alternative allele are colored navy.

**S12 Fig. Linkage mapping summary for drug-response traits in response to four heavy metals.** Genomic positions (x-axis) of all QTL identified from linkage mapping are shown for each drug-trait (y-axis). Each QTL is plotted as a triangle at the genomic location of the peak marker and a line that represents the 95% confidence interval. QTL with right side up triangles have a negative effect size (N2 allele is resistant), and QTL with upside down triangles have a positive effect size (CB4856 allele is resistant). QTL are colored by the logarithm of the odds (LOD) score, increasing in significance from purple to green to yellow.

**S1 File. Dose response phenotype data.** Processed phenotype data from zinc dose response (standard HTA)

**S2 File. Zinc response heritability.** Phenotypic values and used to calculate heritability and calculated heritabilities for all four zinc response traits (standard HTA)

**S3 File. RIAIL phenotype data.** Phenotypic values for all 121 set 1 RIAILs, 253 set 2 RIAILs, and parent strains (N2 and CB4856) in response to zinc (standard HTA)

**S4 File. Linkage mapping results.** Linkage mapping LOD scores at 13,003 genomic markers for all four zinc-response traits with the set 2 RIAILs

**S5 File. Summary of two-dimensional genome scan.** Summary of the scan2 object containing data from the two-dimensional genome scan with animal optical density (median.EXT) in zinc

**S6 File. List of zinc-related genes.** List of all previously known zinc genes (zinc transporters and hits from mutant screens), their location in the genome, and if they have variation in CB4856

**S7 File. NIL sequence data.** VCF from the whole-genome sequencing for all the NILs in this study

**S8 File. NIL genotype data.** Simplified genotypes of the NILs in the study

**S9 File. NIL phenotype data.** Raw pruned phenotypes for the NILs on chromosomes III, IV, V, and X (standard HTA).

**S10 File. Statistical significance for NIL and CRISPR assays.** Pairwise statistical significance for all strains and high-throughput assays

**S11 File. ChrV NIL breakup phenotype data.** Raw pruned phenotypes for the NILs used to break up the QTL interval on chromosome V (standard HTA)

**S12 File. Modified HTA dose response phenotype data.** Raw pruned phenotypes for the parental dose response with the modified HTA

**S13 File. ChrIII dominance assay phenotype data.** Raw pruned phenotypes for the chromosome III dominance assay (modified HTA)

**S14 File. Genes in the chrIII QTL.** List of all genes in the chromosome III interval, their functional descriptions and GO annotations, and if they have variation in CB4856

**S15 File. Expression QTL mapping results for *sqst-5*.** Linkage mapping results for the *sqst-5* expression data obtained with the set 1 RIAILs

**S16 File. Mediation estimates for chrIII QTL.** Mediation estimates for the chromosome III QTL, including *sqst-5*

1149 **S17 File. N2 and CB4856 *sqst-5* deletion phenotype data.** Raw pruned phenotypes for the
1150 *sqst-5* deletions in the parental backgrounds (modified HTA)
1151 **S18 File. NIL *sqst-5* deletion phenotype data.** Raw pruned phenotypes for the *sqst-5* deletions
1152 in the NIL (ECA859) background (modified HTA)
1153 **S19 File. Reciprocal hemizygosity for *sqst-5* phenotype data.** Raw pruned phenotypes for the
1154 reciprocal hemizygosity assay using the *sqst-5* deletions in the NIL background (modified HTA)
1155 **S20 File. Sequence of *sqst-5* in N2 and CB4856.** Raw sequence of *sqst-5* for both N2 and
1156 CB4856
1157 **S21 File. *sqst-5* gene alignment.** Nucleotide alignment of *sqst-5* for N2 and CB4856
1158 **S22 File. SQST-5 protein alignment.** Protein alignment of SQST-5 for N2 and CB4856
1159 **S23 File. Structural variation in *sqst-5* in 328 wild isolates.** List of all 328 wild isolates, their
1160 isolation location, and extent of structural variation in *sqst-5*
1161 **S24 File. *sqst-5* phylogenetic tree.** Neighbor-joining tree for all 328 wild isolates using variants
1162 near *sqst-5*
1163 **S25 File. Wild isolate phenotype data.** Residual phenotypic values for all 81 wild isolates in
1164 response to zinc (standard HTA)
1165 **S26 File. GWA mapping results.** GWA mapping significance values for all markers across the
1166 genome for all four zinc-response traits
1167 **S27 File. Heavy metals linkage mapping results.** Linkage mapping LOD scores at 13,003
1168 genomic markers for all four metal-response traits with the set 2 RIAILs for four heavy metals